



## A New Class of Bi- and Trifunctional Sugar Oximes as Antidotes against Organophosphorus Poisoning

Ophélie da Silva, Nicolas Probst, Christophe Landry, Anne-Sophie Hanak, Pierre Warnault, Caroline Coisne, André-Guilhem Calas, Fabien Gosselet, Charlotte Courageux, Anne-Julie Gastellier, et al.

### ► To cite this version:

Ophélie da Silva, Nicolas Probst, Christophe Landry, Anne-Sophie Hanak, Pierre Warnault, et al.. A New Class of Bi- and Trifunctional Sugar Oximes as Antidotes against Organophosphorus Poisoning. *Journal of Medicinal Chemistry*, 2022, 65 (6), pp.4649-4666. 10.1021/acs.jmedchem.1c01748 . hal-03706969

HAL Id: hal-03706969

<https://univ-artois.hal.science/hal-03706969>

Submitted on 19 Jul 2022

**HAL** is a multi-disciplinary open access archive for the deposit and dissemination of scientific research documents, whether they are published or not. The documents may come from teaching and research institutions in France or abroad, or from public or private research centers.

L'archive ouverte pluridisciplinaire **HAL**, est destinée au dépôt et à la diffusion de documents scientifiques de niveau recherche, publiés ou non, émanant des établissements d'enseignement et de recherche français ou étrangers, des laboratoires publics ou privés.

# **A new class of bi and trifunctional sugar oximes as antidotes against organophosphorus poisoning.**

4 Ophélie Da Silva<sup>1</sup>, Nicolas Probst<sup>2</sup>, Christophe Landry<sup>3</sup>, Anne-Sophie Hanak<sup>1</sup>, Pierre  
5 Warnault<sup>2</sup>, Caroline Coisne<sup>3</sup>, André-Guilhem Calas<sup>1</sup>, Fabien Gosselet<sup>3</sup>, Charlotte Courageux<sup>1</sup>,  
6 Anne-Julie Gastellier<sup>1</sup>, Marilène Trancart<sup>1</sup>, Rachid Baati<sup>4</sup>, Marie-Pierre Dehouck<sup>3</sup>, Ludovic  
7 Jean<sup>2\*</sup>, Florian Nachon<sup>1</sup>, Pierre-Yves Renard<sup>2</sup> and José Dias<sup>1\*</sup>

## 8 Affiliations

- 9• <sup>1</sup>Département de Toxicologie et Risques Chimiques, Institut de Recherche Biomédicale des  
10 Armées, F-91220 Brétigny-sur-Orge, France.  
11• <sup>2</sup>Normandie Université, COBRA, UMR 6014 & FR 3038, Université de Rouen, INSA Rouen,  
12 CNRS, 1 rue Tesnière, 76821 Mont-Saint-Aignan Cedex, France.  
13• <sup>3</sup>Université d'Artois (UArtois), UR 2465, LBHE Laboratoire de la Barrière Hémato-  
14 Encéphalique, F-62307 Lens, France.  
15 <sup>4</sup>UMR CNRS 7515, ICPEES Institut de Chimie et Procédés pour l'Énergie, l'Environnement  
16 et la Santé, F-67087 Strasbourg, France.  
17 \* Correspondence: [jose.dias@def.gouv.fr](mailto:jose.dias@def.gouv.fr); [ludovic.jean@univ-rouen.fr](mailto:ludovic.jean@univ-rouen.fr)

19 Abstract

Recent events demonstrated that organophosphorus nerve agents are a serious threat for civilian and military populations. The current therapy includes a pyridinium aldoxime reactivator to restore the enzymatic activity of acetylcholinesterase located in the central nervous system and neuro-muscular junctions. One major drawback of these charged acetylcholinesterase reactivators is their poor ability to cross the blood-brain barrier to reach the centrally inhibited enzymes. Many strategies have been evaluated over the years to overcome this weakness. In this study, we propose to evaluate glucoconjugated oximes devoid of permanent charge as potential central nervous system reactivators. We determined their *in vitro* reactivation efficacy on organophosphorus inhibited human acetylcholinesterase and the crystal structure of two compounds in complex with the enzyme. We also determined their protective index on intoxicated mice as well as their pharmacokinetics. In order to gain a fine understanding of our compounds trafficking through the blood-brain barrier, we evaluated the endothelial

32 permeability coefficients of our molecules with a human *in vitro* model. This study shed light  
33 on the structural restraints of new sugar oximes designed to reach the central nervous system  
34 through the active glucose transporter located at the blood-brain barrier.

35 **1. Introduction**

36 The recent use of organophosphorus nerve agents (OPNAs) such as VX against Kim Jong-Nam  
37 in Malaysia in 2017<sup>1</sup> or Novichoks in march 2018 against a former Russian spy, Sergei Skripal  
38 and his daughter Yulia<sup>2</sup> demonstrates that these compounds are still a real threat for the civilian  
39 and military populations. Commonly, nerve agents affect the cholinergic neurotransmission by  
40 phosphorylation of the catalytic serine residue of acetylcholinesterase (AChE, EC 3.1.1.7), a key  
41 enzyme for nerve impulse termination, located in the central nervous system (CNS) and at the  
42 neuromuscular junctions. This covalent binding leads to the irreversible inhibition of the  
43 enzyme, accumulation of the neurotransmitter acetylcholine, and subsequently to a cholinergic  
44 crisis characterized by nausea, dyspnea, seizure and death if not treated rapidly<sup>3</sup>. The current  
45 therapy for OPNAs poisoning associates a muscarinic antagonist drug (e.g. atropine), an  
46 anticonvulsant drug (e.g. diazepam) and a pyridinium aldoxime reactivator (pralidoxime,  
47 trimedoxime, obidoxime, HI-6)<sup>4</sup> able to remove the phosphoryl group attached to the catalytic  
48 serine residue. These permanently charged quaternary oximes present an adequate pKa for the  
49 nucleophilic oxime residue increasing its nucleophilic character, and an electron deficient  
50 heteroaromatic moiety responsible for their binding affinity, and their positioning close to the  
51 phosphorylated serine residue in the enzyme catalytic site. However, these charged oximes are  
52 known cross the blood-brain barrier (BBB) poorly. Thus, if this medical countermeasure can  
53 limit the deadly peripheral cholinergic crisis, they do not reactivate cholinesterases of the CNS,  
54 causing long-lasting neurological disorders and side effects<sup>5</sup>. Only 4 to 10 % of the oxime  
55 present in the plasma cross the BBB and are subsequently available for brain protection against  
56 OP poisoning<sup>6</sup>. Moreover, despite the synthesis and evaluation of numerous new oximes over

57 the past years, no broad-spectrum oxime able to afford protection against all the main OPNAs  
58 has been identified<sup>7</sup>.

59 In order to facilitate reactivators crossing of the BBB and improve the reactivation efficacy of  
60 new oximes in the CNS, many strategies and new compound designs have been explored.  
61 Amongst the different strategies developed recently, two have drawn our attention<sup>8, 9</sup>.  
62 Reactivators devoid of a permanent charge have been proposed to penetrate more efficiently  
63 the BBB and therefore to be more centrally active. *In vitro* results show an increased efficacy  
64 of these non-quaternary reactivators<sup>10-12</sup>. BBB crossing efficacy of some of these non-  
65 quaternary reactivators has been established<sup>13</sup>, yet *in vivo* experiments did not show so far, a  
66 better protection in the mouse model compared to HI-6<sup>14, 15</sup>. Another strategy to improve BBB  
67 penetration has implied the synthesis of sugar-oxime conjugates<sup>16</sup>. Indeed, the glucose  
68 transporter GLUT-1 located at both sides of the BBB has been shown to potentially facilitate  
69 crossing of this physiological barrier of sugar conjugates<sup>17</sup>. When applied to AChE  
70 reactivators, reports have demonstrated that glucose conjugated-2-PAM attenuates paraoxon-  
71 induced hypothermia in rats, suggesting a central effect<sup>16, 18</sup>.

72 Based on these previous results, herein we report the evaluation of the combination of these  
73 two strategies through the development and evaluation of a new class of uncharged oximes  
74 designed to reach inhibited AChE of the CNS through the glucose transporter GLUT-1 located  
75 at the BBB. Amongst the uncharged oximes evaluated so far, 6- substituted 3-  
76 hydroxypyridinaldoximes have shown the best *in vitro* AChE reactivation efficacy so far, we  
77 synthesized thus multi-functional molecules bearing this 3-hydroxypyridinaldoxime moiety as  
78 a reactivator function attached in position 6 or the pyridine to a sugar (glucose or ribose) aiming  
79 at GLUT-1 facilitated BBB crossing of the glycoconjugate. One of the prerequisites for efficient  
80 AChE reactivation is the ability of the reactivator to bind phosphorylated AChE near the  
81 phosphorylated serine residue. The 3-hydroxypyridinaldoxime moiety displaying a limited

82 affinity for AChE active site, structural studies prompted us to increase the affinity of the sugar-  
83 oximes for the phosphorylated AChE through the introduction of a triazole heterocycle between  
84 the sugar and the 3-hydroxypyridinaldoxime. Accordingly, docking experiments and  
85 previously obtained structures of different ligands bound to AChE have shown that such triazole  
86 moiety could improve binding to the gorge of acetylcholinesterase by stacking with aromatic  
87 amino-acids of the gorge <sup>19, 20</sup>. Binding of the triazole should thus 1) prevent the sugar moiety  
88 to interfere with the reactivation process and 2) increase the reactivator efficacy towards  
89 inhibited enzymes thanks to an increased binding affinity. In this study, we performed an  
90 exhaustive evaluation of these newly designed sugar-oximes. In order to guide the synthetic  
91 efforts, we first investigated the binding properties of the newly designed molecules by  
92 molecular docking. Next, the most promising candidates were synthesized, and we evaluated  
93 their reactivation efficacy on recombinant *h*AChE inhibited by various OPNAs and determined  
94 the crystallographic structures of the complexes formed between two of the synthesized sugar-  
95 oxime conjugates and *h*AChE. Then, we determined the protective index of selected sugar-  
96 oximes on mice exposed to OPNAs and finally, we checked the BBB crossing abilities of these  
97 new sugar-oximes molecules with an *in vitro* model mimicking the human BBB. Analysis of  
98 these findings allowed us to shed new light on the different issues associated with BBB crossing  
99 by such chemical counter-measures against OPNAs poisoning and opens the way to the  
100 development of a new family of reactivators.

101 **2. Materials and Methods**

102 **2.1 Chemicals**

103 2-PAM and HI-6 were obtained from Pharmacie Centrale des Armées (Orléans, France), NIMP  
104 (4-nitrophenyl isopropyl methylphosphonate), NEMP (4-nitrophenyl ethyl  
105 methylphosphonate) and NEDPA (4-nitrophenyl ethyl dimethylphosphoramide) from UMR  
106 CNRS 7515 ICPEES (Strasbourg, France). Obidoxime, heparine, DTNB, acetylthiocholine

107 (ATC) and paraoxon were purchased from Sigma-Aldrich (Saint-Quentin-Fallavier, France).  
108 HI-6, 2-PAM, obidoxime (chlorhydrate salts), oxime 4 and 4' were dissolved into physiological  
109 serum (0.9 % NaCl) to obtain the concentration of 10 mM for *in vivo* experiments.

110 **2.2 Chemistry**

111 **General.** Solvents were purified by a dry solvent station MB-SPS-800 (MBraun, Garching,  
112 Germany) immediately prior to use. Triethylamine was distilled from KOH. All reagents were  
113 obtained from commercial suppliers (Sigma-Aldrich, St Quentin Fallavier, France; Acros  
114 Illkirch, France; TCI Europe, Paris, France) unless otherwise stated. The melting points were  
115 recorded on a Stuart SMP30 apparatus (Stuart, Staffordshire, UK). Column chromatography  
116 purifications were performed with prepacked SI-HP (30 µm) or SI-HC (15 µm) columns from  
117 Interchim (Montluçon, France). Preparative normal phase chromatography was carried out on  
118 an automated flash purification apparatus, either Biotage Isolera One (Biotage, Uppsala,  
119 Sweden) or Interchim 420 PuriFlash. Thin-layer chromatography (TLC) was carried out on  
120 Merck DC Kieselgel 60F-254 aluminum sheets (Merck, Darmstadt, Germany). Compounds  
121 were visualized by UV irradiation and/or spraying with a solution of vanillin, followed by  
122 smooth heating. <sup>1</sup>H and <sup>13</sup>C NMR spectra were recorded with a Bruker DPX 300 spectrometer  
123 (Bruker, Wissembourg, France) and are presented in the Supporting Information (S9, NMR  
124 spectra). Chemical shifts are expressed in parts per million (ppm) from CDCl<sub>3</sub> ( $\delta$ H = 7.26 ppm,  
125  $\delta$ C = 77.16 ppm). *J* values are expressed in hertz. Mass spectra were obtained with a Finnigan  
126 LCQAdvantage MAX (ion trap) apparatus equipped with an electrospray source (Thermo  
127 Electron Corporation, Waltham, MA). High-resolution mass spectra were obtained with a  
128 Varian MAT 311 spectrometer (Varian MAT, Bremen, Germany) using electrospray analysis.  
129 HPLC quality grade acetonitrile and Milli-Q purified water were used for analytical and  
130 preparative HPLC. Preparative HPLC run was carried out with an Interchim 4250 apparatus  
131 (Interchim, Montluçon, France) with an Interchim puriflash C18 column (Interchim,

132 Montluçon, France), 30 × 250 mm, C18AQ-5 µm. Analytical HPLC was performed on a  
133 ThermoFisher UHPLC Ultimate 3000 instrument (Thermofisher, Waltham, MA) equipped with  
134 a PDA detector under the following conditions: Syncronis C18 column (3 µm, 3 × 100 mm)  
135 with MeCN and 20 mM NH<sub>4</sub>OAc as eluents [using a gradient from 100% 20 mM NH<sub>4</sub>OAc to  
136 100% MeCN over 30 min] at a flow rate of 0.5 mL/min with UV detection at 254 nm. The  
137 synthesis of oxime 1, 2, 3, 4, 4', 5 and 15 are described below. The general chemistry,  
138 experimental information, and syntheses of all other compounds are supplied in the Supporting  
139 Information. The purity of all final compounds as determined by HPLC analysis is ≥ 95 %. The  
140 canonical SMILES of all compounds tested are provided in Table S1.

141 **(E)-3-hydroxy-6-((2*R*,3*R*,4*S*,5*S*,6*R*)-3,4,5-trihydroxy-6-(hydroxymethyl)tetrahydro-**  
142 **2*H*-pyran-2-yl)oxybutyl)picolinaldehyde oxime 1**

143 General procedure of oxime formation/deacetylation applied on aldehyde **47** (496 mg, 0.94  
144 mmol). The residue was purified by preparative HPLC (0 % for 5 min then 0 % to 30% MeCN  
145 in H<sub>2</sub>O over 25 min then 30% to 100% over 5 min, 40 mL/min, Interchim puriflash prep  
146 C18AQ, 30x250 mm, 5 micro, PF5C18AQ-250/300) to afford the title compound as a solid  
147 (137 mg, 39%). mp = 47–53 °C.  $[\alpha]_D^{20} = -22.8$  (c 0.50 MeOH). <sup>1</sup>H NMR (300 MHz, MeOD):  
148 δ 8.31 (s, 1H), 7.29 (d, *J* = 8.5 Hz, 1H), 7.19 (d, *J* = 8.5 Hz, 1H), 4.27 (d, *J* = 7.8 Hz, 1H), 3.96  
149 (dt, *J* = 9.6, 6.4 Hz, 1H), 3.88 (dd, *J* = 11.9, 2.0 Hz, 1H), 3.72 – 3.64 (m, 1H), 3.59 (dt, *J* = 9.6,  
150 6.3 Hz, 1H), 3.41 – 3.25 (m, 3H), 3.19 (dd, *J* = 8.9, 7.7 Hz, 1H), 2.81 – 2.72 (m, 2H), 1.87 –  
151 1.73 (m, 2H), 1.73 – 1.61 (m, 2H). <sup>13</sup>C NMR (75 MHz, MeOD): δ 153.3, 152.4, 151.4, 134.8,  
152 124.7, 124.0, 103.0, 76.7, 76.5, 73.7, 70.3, 69.0, 61.4, 36.1, 28.8, 26.3. HRMS (ESI<sup>+</sup>): m/z  
153 calculated for [C<sub>16</sub>H<sub>25</sub>N<sub>2</sub>O<sub>8</sub>]<sup>+</sup> 373.1611, found 373.1608.

154 **(E)-3-hydroxy-6-((2*R*,3*R*,4*S*,5*S*,6*R*)-3,4,5-trihydroxy-6-(hydroxymethyl)tetrahydro-**  
155 **2*H*-pyran-2-yl)oxypropyl)picolinaldehyde oxime 2**

156 General procedure of oxime formation/deacetylation applied on aldehyde **46** (336 mg, 0.98  
157 mmol). The residue was purified by preparative HPLC (0% for 5 min then 0 % to 40% MeCN  
158 in H<sub>2</sub>O over 25 min then 30% to 100% over 5 min, 40 mL/min, Interchim puriflash prep  
159 C18AQ, 30x250 mm, 5 micro, PF5C18AQ-250/300) to afford the title compound as an oil (143  
160 mg, 41%).  $[\alpha]_D^{20} = -18.0$  (*c* 0.50 MeOH). <sup>1</sup>H NMR (300 MHz, MeOD):  $\delta$  8.32 (s, 1H), 7.29  
161 (d, *J* = 8.5 Hz, 1H), 7.22 (d, *J* = 8.5 Hz, 1H), 4.27 (d, *J* = 7.7 Hz, 1H), 3.94 (dt, *J* = 9.6, 6.1 Hz,  
162 1H), 3.91 – 3.84 (m, 1H), 3.69 (dd, *J* = 11.9, 5.1 Hz, 1H), 3.58 (dt, *J* = 9.8, 6.4 Hz, 1H), 3.43 –  
163 3.25 (m, 4H), 3.22 (dd, *J* = 8.9, 7.7 Hz, 1H), 2.85 (dd, *J* = 8.6, 6.7 Hz, 2H), 2.07 – 1.91 (m, 2H).  
164 <sup>13</sup>C NMR (75 MHz, MeOD):  $\delta$  152.9, 152.4, 151.5, 134.9, 124.7, 124.2, 103.1, 76.7, 76.5, 73.8,  
165 70.3, 68.4, 61.4, 32.8, 29.9. HRMS (ESI<sup>+</sup>): m/z calculated for [C<sub>15</sub>H<sub>23</sub>N<sub>2</sub>O<sub>8</sub>]<sup>+</sup> 359.1454, found  
166 359.1458.

167 **(E)-3-hydroxy-6-(3-(4-((2R,3R,4S,5S,6R)-3,4,5-trihydroxy-6-**  
168 **(hydroxymethyl)tetrahydro-2H-pyran-2-yl)oxy)butyl)-1H-1,2,3-triazol-1-**  
169 **yl)propyl)picolinaldehyde oxime 3**

170 General procedure of oxime formation/deacetylation applied on aldehyde **48** (677 mg, 1.07  
171 mmol). The residue was purified by normal phase flash chromatography (10% to 30% MeOH  
172 in DCM over 30 min, 12G SIHC) then reversed-phase flash chromatography (5 to 60% MeCN  
173 in H<sub>2</sub>O over 30 min, 80 G, C18-15 micro, Interchim) to afford an off-white solid (384 mg,  
174 75%). R<sub>f</sub> = 0.12 (DCM/MeOH 90/10, v/v).  $[\alpha]_D^{20} = -15.3$  (*c* 0.53 MeOH). <sup>1</sup>H NMR (300 MHz,  
175 MeOD):  $\delta$  8.28 (s, 1H), 7.73 (s, 1H), 7.25 (d, *J* = 8.4 Hz, 1H), 7.12 (d, *J* = 8.5 Hz, 1H), 4.87 (s,  
176 7H), 4.41 (t, *J* = 6.9 Hz, 2H), 4.25 (d, *J* = 7.8 Hz, 1H), 3.94 (dt, *J* = 9.6, 6.3 Hz, 1H), 3.86 (dd,  
177 *J* = 11.9, 1.9 Hz, 1H), 3.67 (dd, *J* = 11.9, 5.3 Hz, 1H), 3.58 (dt, *J* = 9.6, 6.2 Hz, 1H), 3.39 – 3.32  
178 (m, 1H), 3.32 – 3.24 (m, 1H), 3.28 – 3.25 (m, 1H), 3.18 (dd, *J* = 8.9, 7.7 Hz, 1H), 2.76 – 2.71  
179 (m, 2H), 2.71 (t, *J* = 8.0 Hz, 2H), 2.29 (p, *J* = 6.9 Hz, 2H), 1.84 – 1.69 (m, 2H), 1.69 – 1.56 (m,  
180 2H). <sup>13</sup>C NMR (75 MHz, MeOD):  $\delta$  152.5, 151.6, 151.4, 147.7, 135.2, 124.6, 124.0, 121.9,

181 103.0, 76.7, 76.5, 73.7, 70.3, 68.9, 61.4, 49.3, 33.2, 29.8, 28.7, 25.6, 24.5. HRMS (ESI<sup>+</sup>): m/z  
182 calculated for [C<sub>21</sub>H<sub>31</sub>N<sub>5</sub>O<sub>8</sub>Na]<sup>+</sup> 504.2070, found 504.2072.

183 (*E*)-3-hydroxy-6-(4-(4-((2*R*,3*R*,4*S*,5*S*,6*R*)-3,4,5-trihydroxy-6-  
184 (hydroxymethyl)tetrahydro-2*H*-pyran-2-yl)oxy)butyl)-1*H*-1,2,3-triazol-1-  
185 yl)butyl)picolinaldehyde oxime 4

186 General procedure of oxime formation/deacetylation applied on aldehyde **49** (146 mg, 0.22  
187 mmol). The residue was purified by normal phase flash chromatography (10% to 30% MeOH  
188 in DCM over 30 min, 12G SIHC) then reversed-phase flash chromatography (5 to 100 % MeCN  
189 in H<sub>2</sub>O over 30 min, 80 G, C18-15 micro, Interchim) to afford an oil (112 mg, 100%). R<sub>f</sub> = 0.14  
190 (DCM/MeOH 9/1, v/v). [α]<sub>D</sub><sup>23</sup> = -14.5 (c 0.43 MeOH). <sup>1</sup>H NMR (300 MHz, MeOD): δ 8.26  
191 (s, 1H), 7.74 (s, 1H), 7.26 (d, *J* = 8.4 Hz, 1H), 7.13 (d, *J* = 8.5 Hz, 1H), 4.39 (t, *J* = 6.8 Hz, 2H),  
192 4.26 (d, *J* = 7.7 Hz, 1H), 3.93 (dt, *J* = 9.5, 6.2 Hz, 1H), 3.86 (dd, *J* = 12.1, 1.8 Hz, 1H), 3.67  
193 (dd, *J* = 11.9, 4.8 Hz, 1H), 3.57 (dt, *J* = 9.6, 6.2 Hz, 1H), 3.44 – 3.11 (m, 3H), 3.18 (t, *J* = 8.3  
194 Hz, 1H), 2.74 (t, *J* = 7.7 Hz, 2H), 2.71 (t, *J* = 7.7 Hz, 2H), 2.00 – 1.82 (m, 2H), 1.82 – 1.57 (m,  
195 6H). <sup>13</sup>C NMR (75 MHz, MeOD): δ 153.9, 153.8, 152.7, 149.1, 136.3, 126.1, 125.4, 123.2,  
196 104.3, 78.0, 77.8, 75.1, 71.6, 70.3, 62.7, 51.0, 36.9, 30.7, 30.0, 27.8, 27.0, 25.9. HRMS (ESI<sup>+</sup>):  
197 m/z calculated for [C<sub>22</sub>H<sub>34</sub>N<sub>5</sub>O<sub>8</sub>]<sup>+</sup> 496.2407 found 496.2413.

198 (*E*)-3-hydroxy-6-(4-(4-((2*S*,3*R*,4*S*,5*S*,6*R*)-3,4,5-trihydroxy-6-  
199 (hydroxymethyl)tetrahydro-2*H*-pyran-2-yl)oxy)butyl)-1*H*-1,2,3-triazol-1-  
200 yl)butyl)picolinaldehyde oxime 4'

201 General procedure of oxime formation/deacetylation applied on aldehyde **50** (369 mg, 0.57  
202 mmol). The residue was purified by normal phase flash chromatography (10 to 30% MeOH in  
203 DCM over 30 min, 12G SIHC) then reversed-phase flash chromatography (5 to 100 % MeCN  
204 in H<sub>2</sub>O over 30 min, 80 G, C18-15 micro, Interchim) to afford an oil (225 mg, 80%). [α]<sub>D</sub><sup>26</sup> =  
205 +65.1 (c 0.42 MeOH). <sup>1</sup>H NMR (300 MHz, MeOD): δ 8.28 (s, 1H), 7.75 (s, 1H), 7.28 (d, *J* =

206 8.5 Hz, 1H), 7.14 (d,  $J$  = 8.5 Hz, 1H), 4.78 (d,  $J$  = 3.7 Hz, 1H), 4.40 (t,  $J$  = 6.9 Hz, 2H), 3.81  
207 (dd,  $J$  = 11.7, 2.4 Hz, 2H), 3.86 – 3.71 (m, 1H), 3.67 (dd,  $J$  = 11.7, 5.7 Hz, 1H), 3.66 (dd,  $J$  =  
208 9.7, 8.8 Hz, 1H), 3.58 (ddd,  $J$  = 9.9, 5.6, 2.4 Hz, 1H), 3.48 (dt,  $J$  = 9.7, 5.9 Hz, 1H), 3.40 (dd,  $J$   
209 = 9.7, 3.7 Hz, 1H), 3.29 (dd,  $J$  = 9.8, 8.8 Hz, 1H), 2.76 (t,  $J$  = 7.7 Hz, 2H), 2.74 (t,  $J$  = 7.7 Hz,  
210 2H), 1.99 – 1.87 (m, 2H), 1.84 – 1.61 (m, 6H).  $^{13}\text{C}$  NMR (75 MHz, MeOD):  $\delta$  153.9, 153.8,  
211 152.9, 149.0, 136.4, 126.0, 125.3, 123.2, 100.1, 75.2, 73.7, 73.6, 71.9, 68.6, 62.8, 51.0, 37.0,  
212 30.7, 29.9, 27.9, 27.2, 26.0. HRMS (ESI $^+$ ): m/z calculated for [C<sub>22</sub>H<sub>34</sub>N<sub>5</sub>O<sub>8</sub>] $^+$  496.2407, found  
213 496.2399.

214 (*E*)-6-(4-(4-(((2*R*,3*R*,4*S*,5*R*)-3,4-dihydroxy-5-(hydroxymethyl)tetrahydrofuran-2-  
215 yl)oxy)butyl)-1*H*-1,2,3-triazol-1-yl)butyl)-3-hydroxypicolinaldehyde oxime **5**

216 General procedure of oxime formation/deacetylation applied on aldehyde **51** (398 mg, 0.69  
217 mmol). The residue was purified by normal phase flash chromatography (5 to 30% MeOH in  
218 DCM over 30 min, 25G SIHC), then purified by preparative HPLC (0% for 5 min, then 0 to  
219 40% MeCN in H<sub>2</sub>O over 30 min, puriflash C18, 30x250 mm, C18AQ-5 micro) to afford the  
220 title compound as an oil (233 mg, 73%).  $R_f$  = 0.13 (DCM/MeOH 9/1, v/v).  $[\alpha]_D^{24} = -21.1$  (c  
221 0,53 MeOH).  $^1\text{H}$  NMR (300 MHz, MeOD):  $\delta$  8.14 (s, 1H), 7.59 (s, 1H), 7.13 (d,  $J$  = 8.4 Hz,  
222 1H), 6.99 (d,  $J$  = 8.4 Hz, 1H), 4.73 (d,  $J$  = 4.0 Hz, 1H), 4.26 (t,  $J$  = 6.9 Hz, 2H), 3.92 (dd,  $J$  =  
223 6.9, 4.7 Hz, 1H), 3.82 (td,  $J$  = 6.7, 3.5 Hz, 1H), 3.76 (dd,  $J$  = 4.7, 1.0 Hz, 1H), 3.71 – 3.57 (m,  
224 1H), 3.60 (dd,  $J$  = 11.8, 3.6 Hz, 1H), 3.42 (dd,  $J$  = 11.7, 6.5 Hz, 1H), 3.28 (dt,  $J$  = 9.5, 6.2 Hz,  
225 1H), 2.62 (t,  $J$  = 6.5 Hz, 2H), 2.59 – 2.51 (m, 2H), 1.78 (dd,  $J$  = 15.0, 7.5 Hz, 2H), 1.66 – 1.39  
226 (m, 6H).  $^{13}\text{C}$  NMR (75 MHz, MeOD):  $\delta$  152.5, 152.4, 151.5, 147.6, 135.0, 124.6, 123.9, 121.8,  
227 107.4, 83.4, 74.9, 71.4, 67.0, 63.7, 49.6, 35.6, 29.3, 28.7, 26.5, 25.8, 24.6. HRMS (ESI $^+$ ): m/z  
228 calcd for [C<sub>21</sub>H<sub>32</sub>N<sub>5</sub>O<sub>7</sub>] $^+$  466.2302, found 466.2303.

229 (*E*)-6-((2*R*,3*R*,4*S*,5*R*)-3,4-dihydroxy-5-(hydroxymethyl)tetrahydrofuran-2-  
230 yl)oxy)hexyl)-3-hydroxypicolinaldehyde oxime **15**

231 General procedure of oxime formation/deacetylation applied on aldehyde **52** (318 mg, 0.66  
232 mmol). The residue was purified by normal phase flash chromatography (5 to 30% MeOH in  
233 DCM over 30 min, 25G SIHC), then purified by preparative HPLC (5 to 50% MeCN in H<sub>2</sub>O  
234 over 30 min, puriflash C18, 30x250 mm, C18AQ-5 micro) to afford the title compound as an  
235 oil (128 mg, 52%). R<sub>f</sub> = 0.22 (90/10 DCM/MeOH, v/v). [α]<sub>D</sub><sup>20</sup> = - 26.3(c 0.51 MeOH). <sup>1</sup>H  
236 NMR (300 MHz, CDCl<sub>3</sub>): δ 8.29 (s, 1H), 7.27 (d, J = 8.5 Hz, 1H), 7.15 (d, J = 8.5 Hz, 1H),  
237 4.83 (s, 1H), 4.03 (dd, J = 6.9, 4.7 Hz, 1H), 3.93 (td, J = 6.7, 3.5 Hz, 1H), 3.87 (d, J = 4.7 Hz,  
238 1H), 3.79 – 3.65 (m, 2H), 3.54 (dd, J = 11.7, 6.6 Hz, 1H), 3.36 (dt, J = 9.3, 6.3 Hz, 1H), 2.71  
239 (dd, J = 8.7, 6.7 Hz, 2H), 1.67 (h, J = 7.2 Hz, 2H), 1.54 (q, J = 6.6 Hz, 2H), 1.37 (h, J = 5.5, 4.5  
240 Hz, 4H). <sup>13</sup>C NMR (75 MHz, CDCl<sub>3</sub>): δ 154.8, 153.8, 152.8, 136.2, 126.1, 125.3, 108.7, 84.7,  
241 76.3, 72.8, 68.8, 65.2, 37.8, 31.3, 30.6, 30.1, 27.1. HRMS (ESI<sup>+</sup>): m/z calculated for  
242 [C<sub>17</sub>H<sub>27</sub>N<sub>2</sub>O<sub>7</sub>]<sup>+</sup> 371.1818, found 371.1824.

243 **2.3 Molecular docking**

244 Flexible dockings with the newly designed sugar-oxime conjugates have been performed using  
245 AutoDock Vina <sup>21</sup> as described previously <sup>22</sup> with the receptor files for GB-*hAChE* and VX-  
246 *hAChE*. For each phosphorylated *hAChE*, 10 poses per oxime were generated and the best  
247 identified poses were determined based on the minimal distance between the oxygen atom of  
248 the oxime and the phosphorus atom of the OP serine conjugated and by the higher binding  
249 affinity achieved.

250 **2.4 Recombinant human acetylcholinesterase**

251 Recombinant *hAChE* was produced and purified as previously described <sup>23</sup>.

252 **2.5 Phosphylation of recombinant human acetylcholinesterase**

253 Stock solutions of OPNAs surrogates (NIMP as sarin surrogate, NEMP as VX surrogate and  
254 NEDPA as Tabun surrogate) or VX at 5 mM in isopropanol were used to inhibit the purified  
255 *hAChE* as previously described <sup>24</sup>. It is worth noting that using the OPNA surrogates gives the

256 same phosphoryl residue than the real OP, and thus the same phosphorylated AChE. Briefly, a ten-  
257 fold excess of OPNA surrogates or VX was used to perform the inhibition of *h*AChE in a  
258 sodium phosphate buffer (100 mM, pH 7.4, 0.1% BSA) at 25°C. Complete inhibition of *h*AChE  
259 was monitored by measuring the residual activity with a modified Ellman assay as previously  
260 described <sup>25</sup> and excess of OPNAs surrogates or VX were removed using a desalting PD-10  
261 column (GE Healthcare).

262 **2.6 IC<sub>50</sub> measurements**

263 Oximes were dissolved in methanol to prepare a 40 mM stock solution and subsequently diluted  
264 in water to reach the desired concentrations. Recombinant *h*AChE activity was measured in a  
265 buffer containing 0,1 M phosphate buffer pH 7.4 / 0.1 % BSA / 0.1 mg/ml DTNB / 1 mM ATC  
266 and in presence of various oximes concentrations using a modified Ellman assay <sup>25</sup> measuring  
267 the released thiophenol concentration through the UV/Vis absorbance at 412 nm and 25°C.  
268 Measurements were performed at least in duplicate for each tested concentration and final  
269 methanol concentrations were kept below 5%. The compound concentration producing 50 %  
270 inhibition was determined by nonlinear fitting with ProFit (Quantumsoft) using the standard  
271 IC<sub>50</sub> equation:

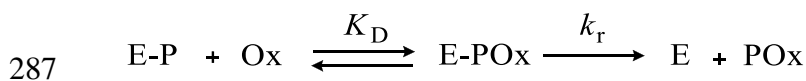
$$272 \quad \% \text{ activity} = \frac{100 \times IC_{50}}{(IC_{50} + [Cp])}$$

273  
274

275 **2.7 In vitro reactivation of phosphorylated human acetylcholinesterase**

276 The reactivation of OPNAs-inhibited *h*AChE was performed as previously described <sup>15</sup>. Briefly,  
277 the phosphorylated enzymes were incubated at 37°C with various concentrations of oximes in 0,1  
278 % BSA / 0,1 M phosphate buffer pH 7.4. Final concentration of methanol was kept below 2 %  
279 and had no effect on enzyme activity. Aliquots of the reactivation mixture were transferred at  
280 different time interval to cuvettes containing 1 mM ATC in 1 mL of Ellman's buffer (0.5 mM  
281 DTNB in 0.1 M sodium phosphate buffer, pH 7.4) to measure the *h*AChE activity through the

283 evaluation of the amount of thiophenol obtained by thiocholine cleavage of DTNB through  
284 measurement of its UV-Vis absorption at 412 nm and 25°C. The reactivation constants  $k_{obs}$ ,  $K_D$ ,  
285  $k_r$  and  $k_{r2}$  have been calculated by non-linear fitting of the standard oxime-concentration-  
286 dependent reactivation equation with ProFit (Quantumsoft) derived from the following scheme.



288 
$$k_{obs} = \frac{k_r [O_x]}{K_D + [O_x]} \quad \text{and} \quad k_{r2} = \frac{k_r}{K_D}$$

289

## 290 **2.8 Human Acetylcholinesterase crystallization**

291 Recombinant human acetylcholinesterase crystals were grown using the hanging drop vapor  
292 diffusion method as described previously <sup>23</sup>. Crystals were soaked 60 min in the mother liquor  
293 containing 2 mM of each compound. Crystals were then washed with a cryoprotectant solution  
294 (1.6 M lithium sulfate, 100 mM HEPES pH 7.0, 60 mM magnesium sulfate and 18 % glycerol)  
295 and flash-cooled in liquid nitrogen.

## 296 **2.9 Data collection, reduction and refinement**

297 Diffraction data were collected at the European Synchrotron Radiation Facility (ESRF,  
298 Grenoble, France) at the ID23-2 beam line ( $\lambda = 0.873 \text{ \AA}$ ) and processed with XDS <sup>26</sup> and scaled  
299 with XSCALE. The structure was solved by molecular replacement with PHASER <sup>27</sup> using pdb  
300 4EY4 as starting model, iterative cycles of model building using Coot <sup>28</sup> and refinement using  
301 Phenix <sup>29</sup>. Data collection and refinement statistics are presented in supporting information  
302 (table S2).

## 303 **2.10 Animals**

304 We used 9-week-old male Swiss mice (Janvier Labs, Le Genest-Saint-Isle, France), weighing  
305 35-45 g at the experimentation time. The animals (3-4/cage) were housed for 14-18 days before  
306 the experiments in an environment maintained at  $22 \pm 1^\circ\text{C}$  with controlled humidity on a 12 h

307 dark/light cycle with light provided between 7 a.m. and 7 p.m. They were given food and tap  
308 water *ad libitum*. All experiments were carried out in compliance with the European Directive  
309 on the protection of animals used for scientific purposes (2010/63/UE) and were approved by  
310 our Institutional Animal Care and Research Advisory Committee (approval n°239 of 10-09-  
311 2018).

312 **2.11 Plasma test protocols: monitoring of the reactivability of blood samples**

313 This protocol has been previously fully described <sup>14</sup>.

314 *Standard reactivation curves for pharmacokinetics*

315 Naive mice plasma from Janvier Labs (Le Genest-Saint-Isle, France) was heated at 56°C for 30  
316 min to inactivate endogenous cholinesterases. In a 96-well Greiner plate, VX-phosphylated  
317 *hAChE* solution in sodium phosphate buffer was incubated for 30 min at 37°C in presence of  
318 different concentrations of oximes diluted in heat-inactivated mice plasma (0, 1, 5, 10, 25, 50,  
319 75, 100, 150, 200 and 500 µM). A mix of 2 mM acetylthiocholine and Ellman's buffer (0.5 mM  
320 DTNB in 0.1 M sodium phosphate buffer, pH 7.4, 25°C) was then simultaneously added in all  
321 wells for measurement of resulting *hAChE* activity at 412 nm every 5 s for 30 min with a  
322 SAFAS spectrophotometer (Monaco).

323 The percentage of reactivated enzyme (% E<sub>react</sub>) was calculated as the ratio of the recovered  
324 VX-phosphylated *hAChE* activity and HI-6 reactivated *hAChE* activity, considering that  
325 maximal reactivation (*i.e.*, % E<sub>react</sub> = 100 %) was achieved by incubating VX-phosphylated  
326 *hAChE* with 200 µM HI-6 diluted in heat-inactivated plasma. Standard curves were fitted with  
327 GraphPad Prism software using a simple linear regression.

328 *Blood sampling*

329 Twenty-four hours before the experiment, mice were anesthetized with isoflurane gas  
330 (Vetflurane®, Virbac, France) allowing the shaving of their hind limbs after a 3-min-long  
331 application of a commercial depilatory cream. Then, mice were returned to their cages to allow

332 recovery and complete anesthesia washout. The day of experimentation, mice received  
333 intraperitoneal (i.p.) injection of oxime at 100 µmol/kg by analogy with the previous studies  
334 conducted in our department. At various times (0, 2, 5, 10, 15, 30, 60 and 180 min after oxime  
335 injection), the saphenous vein was drilled with a needle, approximately 20 µL of blood were  
336 collected with a heparinized capillary tube and put in a collection tube containing 2 µL of  
337 sodium heparin (Choay®, Sanofi, France). Plasma was next isolated from erythrocytes by  
338 centrifugation at 4°C, 3 000 g for 10 min. Plasma samples were then heated 30 min at 56°C and  
339 treated as previously described to obtain the percentage of reactivated enzyme (% E<sub>react</sub>) with a  
340 one-compartment model. T<sub>max</sub> corresponds to the time when the curve reaches the peak of %  
341 E<sub>react</sub>. The areas under the percentage of reactivation curve (AUC) and the first moment curve  
342 (AUMC) were calculated using the trapezoidal rule. Mean residence time (MRT) was  
343 calculated as the ratio of AUMC to AUC<sup>30</sup>.

344 **2.12 LD<sub>50</sub> estimation and protective index using the up-and-down method**

345 LD<sub>50</sub> was estimated using the improved method of Dixon's up-and-down procedure described  
346 by Rispin et al.<sup>31</sup>. This method uses an iterative dose-selection algorithm. It consists of a single  
347 ordered dose progression in which mice are dosed, one at a time, at 24 h intervals. The first  
348 animal received a dose a step below the level of the best estimate of the LD<sub>50</sub>. If the mouse  
349 survives, the dose for the next animal is increased by 1.1-fold the original dose; if it dies, the  
350 dose for the next animal is decreased by the same factor. In our particular conditions the testing  
351 stops when one of the following criteria is met: (1) three consecutive animals survive at the  
352 highest dose (which is normally 2000 mg/kg); (2) five reversals occur in any six consecutive  
353 animals tested; (3) at least four animals have followed the first reversal and the specified  
354 likelihood-ratios which compare the maximum likelihood estimate for LD<sub>50</sub> with LD<sub>50</sub> values  
355 above and below exceed the critical value of 2.5. Profile likelihood methods are used to estimate  
356 confidence intervals. In practice the stopping criteria, the resulting LD<sub>50</sub> and the corresponding

357 confidence interval were determined using the AOT 425 Pgm software as recommended by  
358 OECD (7). Antidotal efficacy of the oximes is expressed as a protective index (PI) with 95 %  
359 confidence interval. The PI corresponds to the ratio of LD<sub>50</sub> of the studied OP agent (either  
360 NIMP, NEMP or paraoxon) combined with oxime treatment on LD<sub>50</sub> of OP alone.

361 **2.13 Blood-brain barrier permeability tests**

362 *Human Blood-brain barrier model setting up*

363 The blood-brain barrier (BBB) permeability studies were performed using the *in vitro* human  
364 BBB model previously described and detailed <sup>32</sup>. After infant's parents signed informed  
365 consents, endothelial cells were isolated and differentiated from cord blood CD34<sup>+</sup>-  
366 hematopoietic stem cells according to the protocol described by Pedroso et al. <sup>33</sup> and then  
367 freezed. The preservation and preparation protocol of these cells issued from the human cord  
368 blood were approved by the French Ministry of Higher Education and Research (CODECOH  
369 number DC2011-1321). After thawing within 100 mm petri dishes (Corning, VWR,  
370 Switzerland), the endothelial cells derived from human stem cells reached the confluence and  
371 were then subcultured onto matrigel (BD Biosciences, Franklin Lakes, NJ, USA, 354230)  
372 coated Transwell inserts in the presence of bovine pericytes seeded at bottom of the wells, on  
373 other side of Transwell inserts, to induce the properties of the BBB. Renewal of the medium  
374 [ECM basal medium (ScienCell, Carlsbad, CA, USA) supplemented with 5% (v / v) fetal calf  
375 serum, 1% (v / v) EC growth supplement (ScienCell) and 50 µg / mL gentamycin (Biochrom  
376 AG, Berlin, Germany)] of the co-culture thus set up was carried out every other day. After six  
377 days under these culture conditions, the endothelial cells differentiated in human brain-like  
378 endothelial cells (hBLECs) reproduced characteristics of the *in vivo* BBB <sup>32</sup> and are widely used  
379 to predict molecule toxicity and passage to the CNS <sup>34-37</sup>.

380 *Endothelial permeability coefficient evaluation*

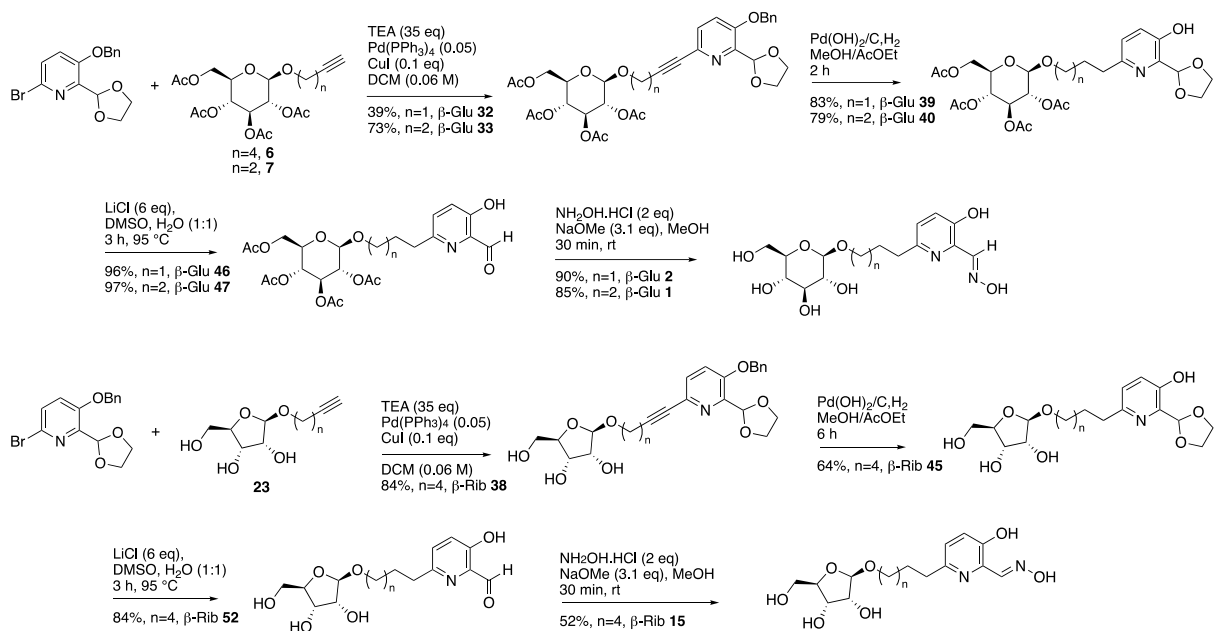
381 The permeability of the BBB to the different oximes and  $^{14}\text{C}$  D-glucose was evaluated by  
382 measuring the endothelial permeability coefficient (Pe) which represents the speed of diffusion  
383 through the BLECs monolayer<sup>38, 39</sup>. Human BLECs monolayers developed after 6 days of  
384 coculture were transferred into new plates containing 1.5 mL per well (abluminal compartment)  
385 of HEPES buffered-Ringer's solution (RH; 150mM NaCl, 5.2mM KCl, 2.2mM NaCl<sub>2</sub>, 0.2mM  
386 MgCl<sub>2</sub>, 6mM NaHCO<sub>3</sub>, 2.8mM glucose, 5mM HEPES). Medium in apical chambers (luminal  
387 compartment) was replaced by 0.5 mL of RH containing either one glycoconjugate oximes or  
388 2-PAM or HI-6 or obidoxime used as oximes control. All compounds were tested at 50 $\mu\text{M}$   
389 (dose checked as non-toxic for the human BLECs) for a diffusion duration of an hour at 37°C.  
390 Then the amount of each oxime in the luminal and abluminal compartments was measured by  
391 mass spectrometry with a TripleTOF 5600+ System (AB SCIEX, Concord, ON, Canada).  
392 Percentages of recovery were checked between 86 and 106%. The quantification of  
393 radiolabeled  $^{14}\text{C}$  D-glucose (PerkinElmer, Boston, MA, USA) was performed using a  
394 scintillation counter TriCarb 2100TR (PerkinElmer, USA).  
395 The clearance principle was used to calculate a concentration-independent permeability  
396 coefficient. The mean compound cleared volume was plotted against time, and the slope was  
397 estimated by linear regression. The permeability values of the inserts (PSf for inserts with a  
398 Matrigel™ coating only) and the inserts with hBLECs (PSt, Matrigel™-coated inserts +  
399 endothelial cells) were taken into consideration by applying the following equation:  $1/\text{PSe} =$   
400  $1/\text{PSt} - 1/\text{PSf}$ . To obtain the endothelial permeability coefficient (Pe expressed in cm/min), the  
401 permeability value (PSe) was divided by the insert's membrane surface area ( $1.13 \text{ cm}^2$ ).

### 402 **3 Results**

#### 403 **3.1 Chemistry**

404 In order to evaluate the requirement of an additional triazole moiety to increase  
405 reactivator affinity with phosphorylated AChE, a first series of 3-

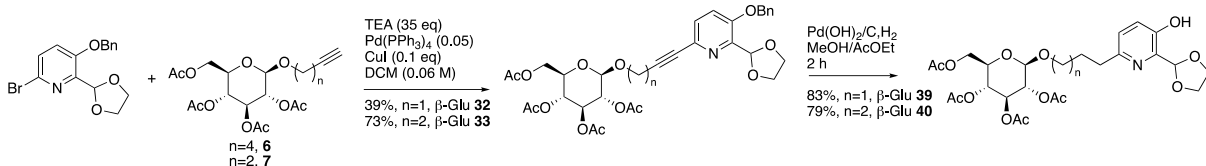
406 hydroxypyridinealdoxime - glucose conjugate was synthesized without the triazole ring.  
 407 The sugar moiety was attached from its anomeric position ( $\beta$  isomer was chosen  
 408 according to the literature describing efficient GLUT-1 mediated BBB crossing using  
 409 such glycoconjugates) to the 6 position of the pyridine ring by an alkyl chain of  
 410 respectively four, three or six carbons, yielding compounds **1**, **2** and **15** in 48%, 28%,  
 411 and 23% yield, respectively, over four steps (



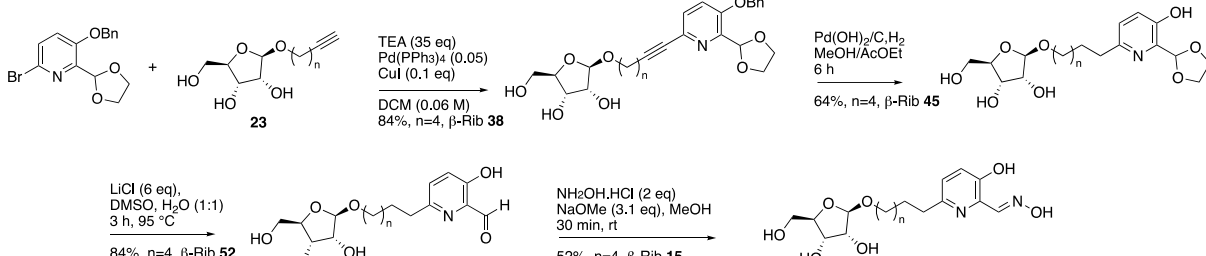
412

413 Figure 1). Peracylated glucose bearing a terminal alkyne moiety at its anomeric position of  
 414 different lengths was obtained as previously described <sup>40</sup>. A Sonogashira cross-coupling  
 415 reaction was used to link the glycosyl moiety and a pre-functionalized pyridine ring using  
 416 standard procedure (CuI, Pd(PPh<sub>3</sub>)<sub>4</sub>) followed by hydrogenation in the presence of Pearlman  
 417 palladium catalyst <sup>41</sup>. Finally, the acetals were removed by a mild and efficient procedure (LiCl  
 418 in DMSO/H<sub>2</sub>O) <sup>42</sup> forming the corresponding 3-hydroxypiconinaldehyde which was converted  
 419 to the aldoxime through reaction with hydroxylamine in methanol. Preparative RP-HPLC  
 420 purified final compounds, and their purity (see 2.1) was determined by RP-HPLC.

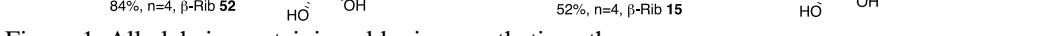
422



423



424



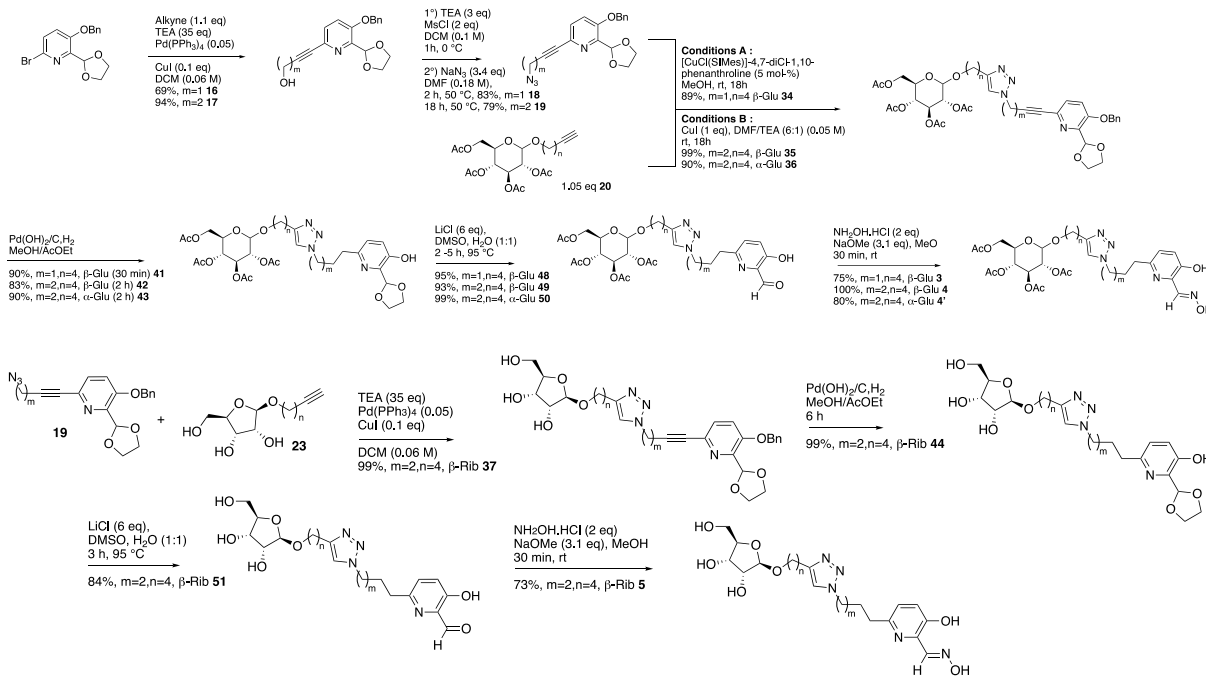
425



426

## Aldoximes 3, 4, 4' and 5 (

427

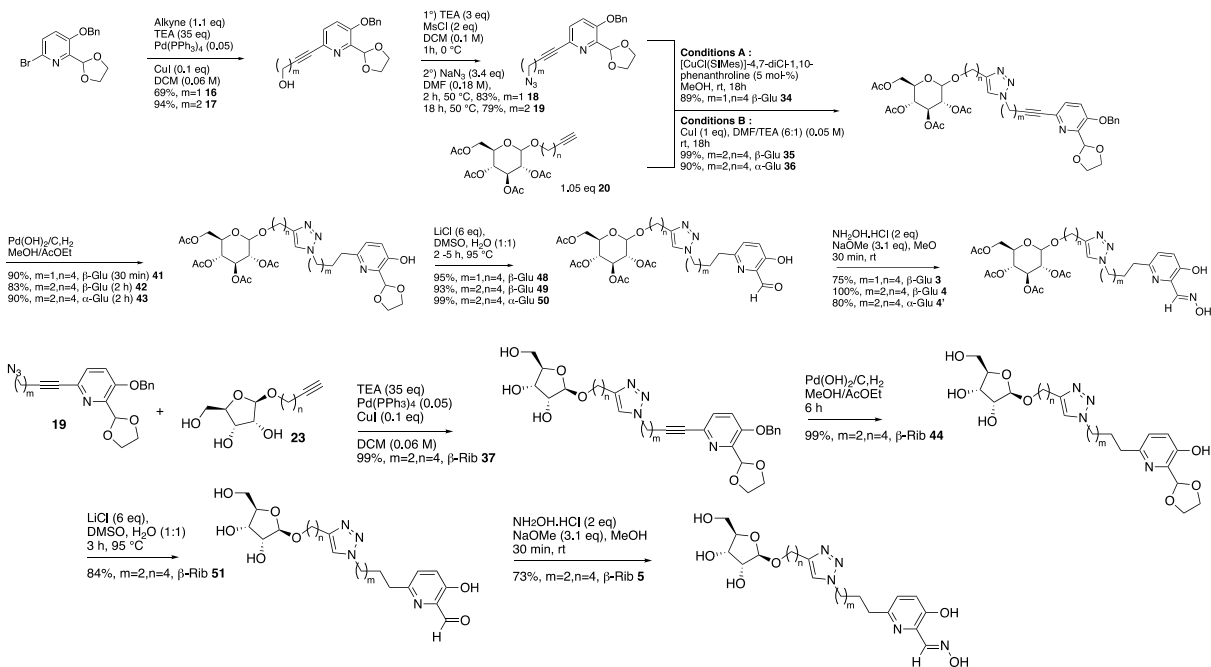


428

429 Figure 2) bearing a triazole heterocycle between the sugar moiety and the position 6 of the  
 430 pyridinaldoxime moiety were obtained using Huisgen cycloaddition between an alkyne chain  
 431 linked to the glycosyl and an azidoalkynylpyridine. Backed by the docking experiments, a 4  
 432 carbons atom linker was found sufficient between the triazole moiety and the sugar to keep the  
 433 sugar moiety away from AChE peripheral site. Docking experiments (vide infra) showed that

434 the best binding affinities were obtained with a 3 or 4 carbon atoms distance between the oxime  
 435 and the triazole ring, thus the  $\beta$ -glucoconjugate **3** and **4** were first targeted. In addition,  $\alpha$ -  
 436 glucoconjugate **4'** and  $\beta$ -riboconjugate **5** were also synthesized to evaluate the role of the sugar  
 437 moiety (glucose vs. ribose) and of the stereochemistry at the anomeric position ( $\alpha$ -glucose vs  
 438  $\beta$ -glucose) in the hexose series. Particular attention was paid to the Huisgen cycloaddition with  
 439 the azidopropynylpyridine which required the use of 5-mol-% of [CuCl(SIMes)]-4,7-dichloro-  
 440 1,10-phenanthroline<sup>43</sup> to avoid by-product formation. The same sequence was used to form the  
 441 oxime moiety (overall yields over the four final steps: 57%, 76%, 64% and 60% respectively  
 442 for **3**, **4**, **4'** and **5**).

443



444

445  
 446

Figure 2. Triazole-containing aldoxime synthetic pathway

447

448 The glycosylation steps were carried out in the presence of either 3-butyn-1-ol, 5-hexyn-1-ol  
 449 as a glycol acceptor and the corresponding glycosyl donor in the form of peracetylated  
 450 glucopyranose or ribofuranose (

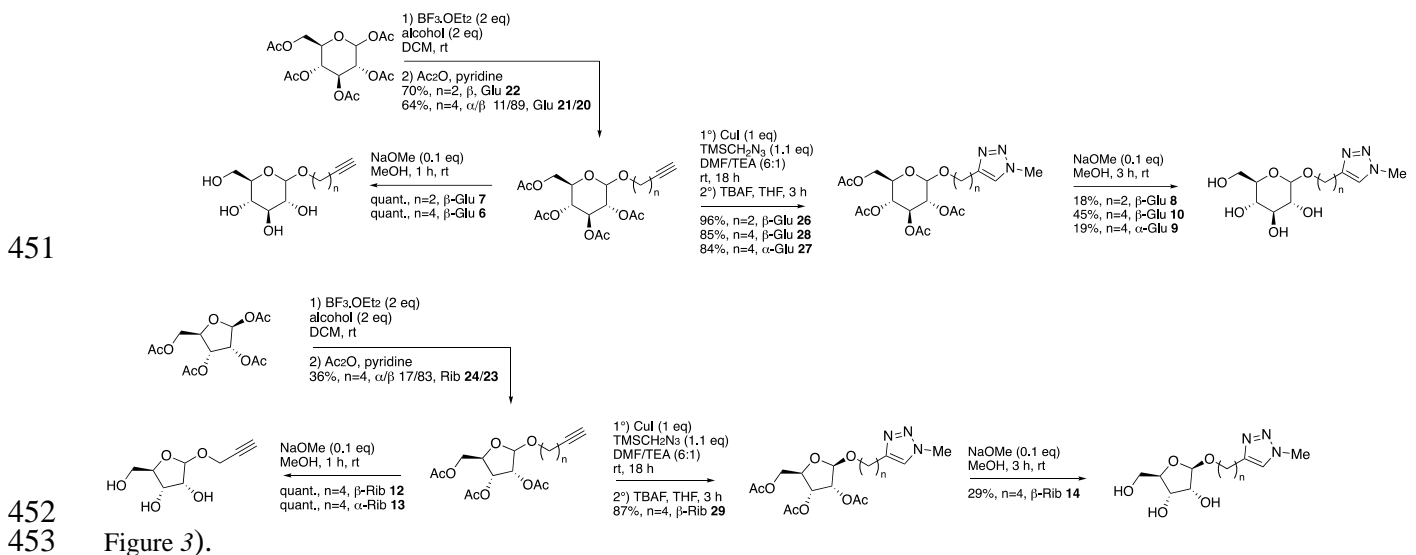


Figure 3).

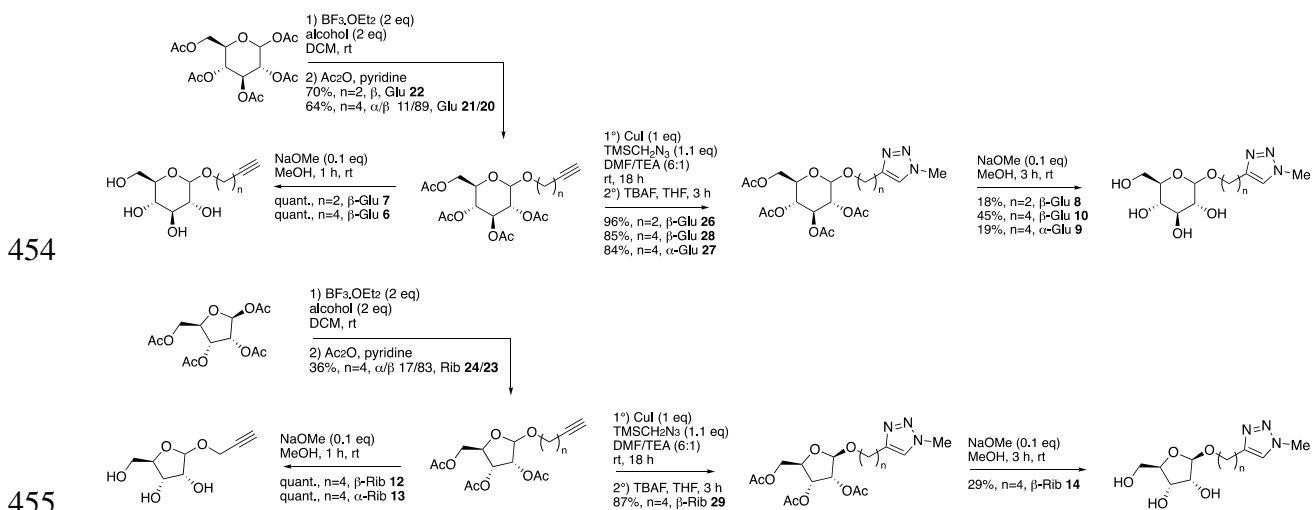
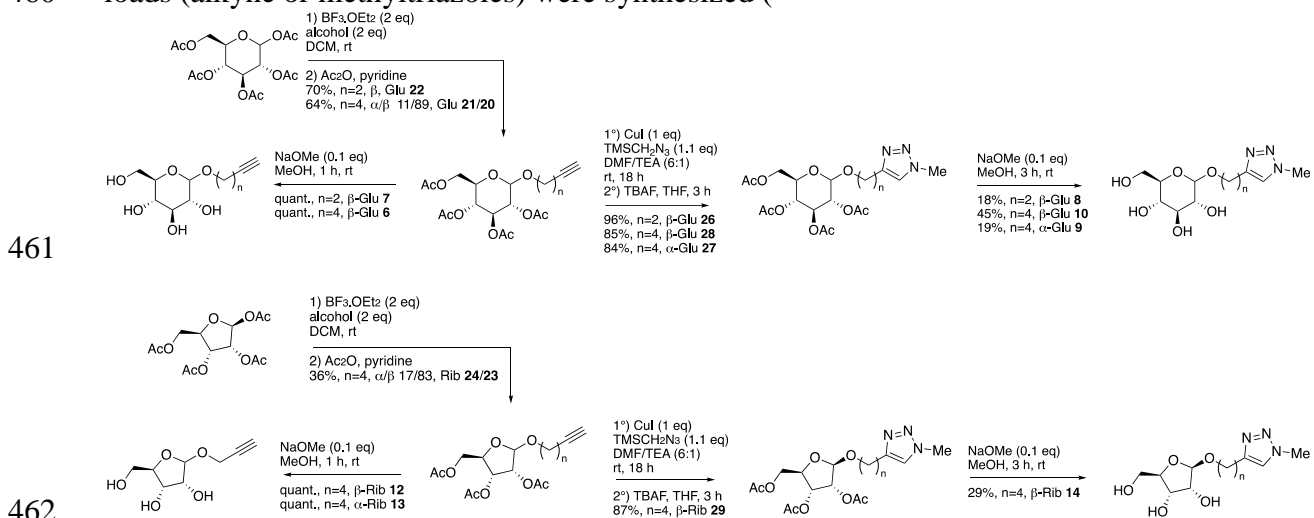


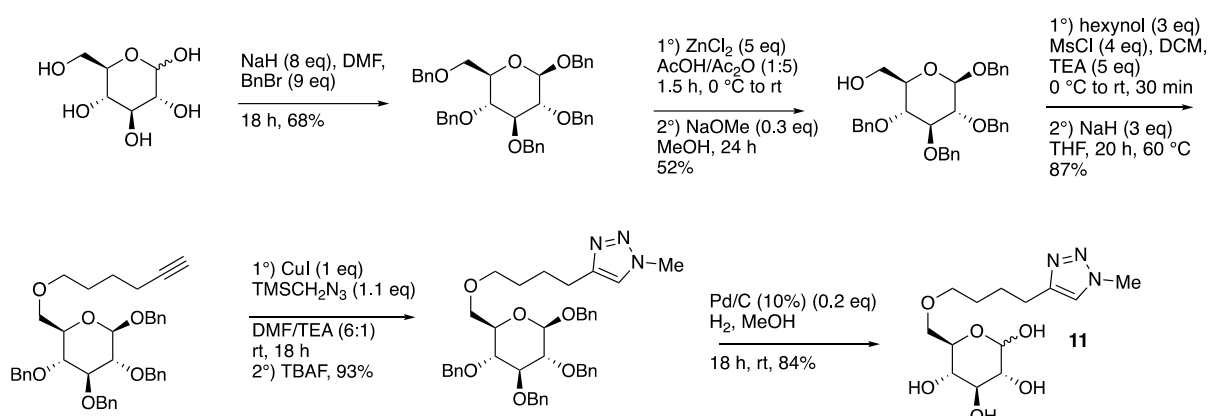
Figure 3. Triazole and alkyne glycoconjugates synthetic pathway

457  
458 In order to gain a better understanding of the glycoconjugate trafficking according to the  
459 sugar derivative, and the glycosyl stereochemistry, several intermediates bearing simpler  
460 loads (alkyne or methyltriazoles) were synthesized (



463 Figure 3). The alkyne chain glycoconjugates **6**, **7**, **12** and **13** were synthesized as a single  
 464 diastereoisomer in two steps from the corresponding peracetylated sugar in respectively 57%,  
 465 70%, 36% and 6% yield by a glycosylation reaction followed by Zemplén procedure to study  
 466 the influence of possible inhibiting interaction. The triazole glycoconjugates, **8**, **9**, **10** and **14**  
 467 were synthesized, as pure diastereoisomer, in 3 steps and respectively in 12%, 1%, 22 % and  
 468 8% overall yields using Huisgen cycloaddition with 1.1 equivalent of trimethylsilylmethyl  
 469 azide followed by TBAF treatment and Zemplén transesterification procedure to uncover the  
 470 *N*-methyltriazole glycoconjugates as free hydroxyl groups.

471 Compound **11**, bearing the triazole alkyl chain on position 6 of the sugar, was also synthesized  
 472 to investigate the impact of the position of the triazole-comprising chain on the BBB  
 473 permeability. Compound **11** was obtained in 5 steps and with 24 % overall yield from glucose.  
 474



475  
 476 Figure 4. Position 6-substituted alkyl-triazole glycoconjugate  
 477

### 3.2 Molecular Docking

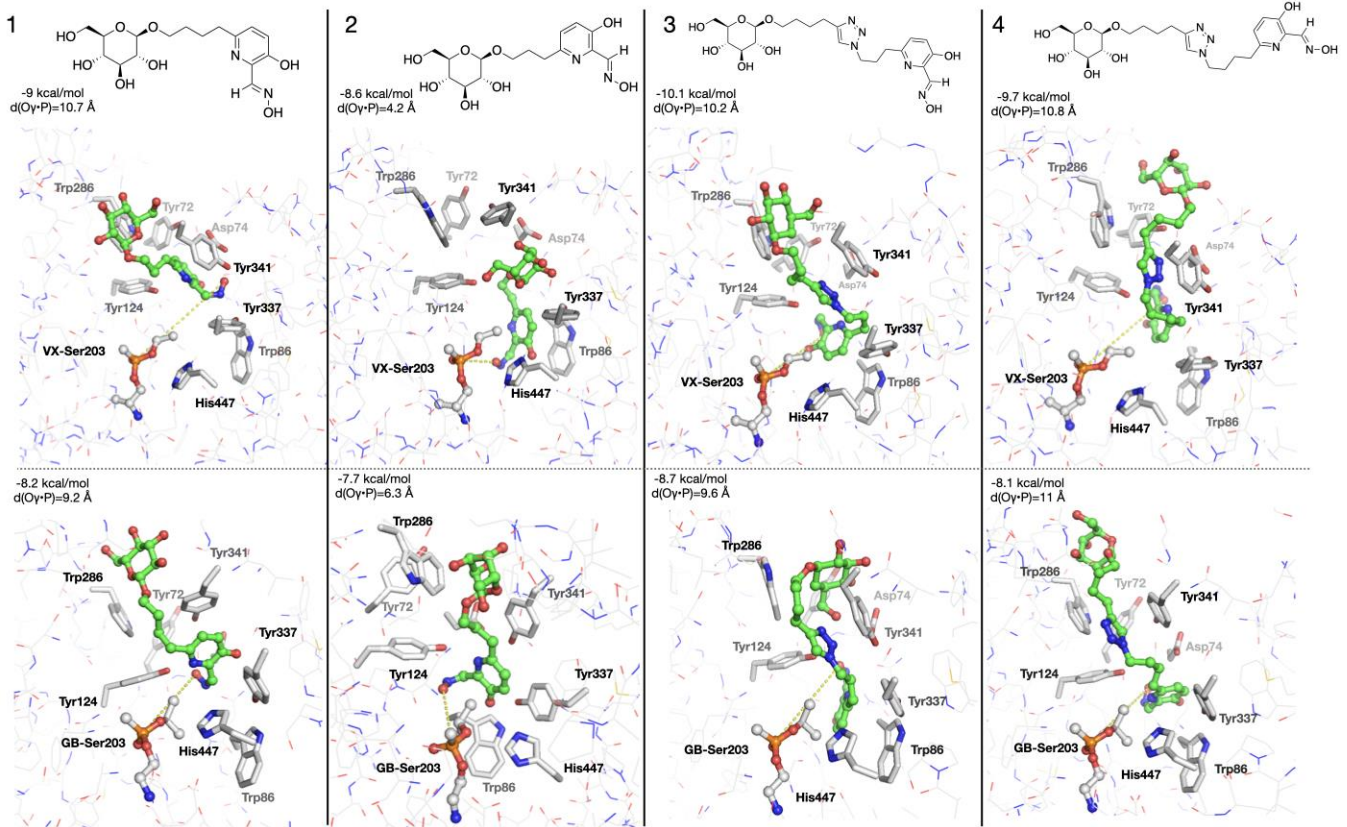
478 To determine if the candidates oximes **1,2,3** and **4** can bind in a productive way to the OPNAs  
 479 phosphorylated *hAChE* close to the catalytic OP-serine adduct, we performed flexible molecular  
 480 docking on *hAChE* phosphorylated by either VX or GB (Sarin) as previously described<sup>22</sup>. The  
 481 side chain of aromatic residues (Trp 286, Tyr72, Tyr341, Tyr124, Tyr337) of the active site of  
 482 *hAChE* as well as the alkoxy chain of the nerve agent were allowed to span freely from their  
 483 native position. The binding energy determined by the scoring function of Autodock Vina and

484 the distances between the phosphorus atoms of nerve agents and the oxime oxygen atom are  
485 reported in table 1.

486 Table 1: Binding affinity and distances between the phosphorus atom of VX and GB-inhibited *hAChE* and the  
487 oxime oxygen atom of the best molecular docking pose of selected oximes. Binding affinity in kcal/mol and P-O  
488 distances in angstrom.

489	490	491	VX		GB		
			Oxime	ΔG (kcal/mol)	Distance P-O (Å)	ΔG (kcal/mol)	Distance P-O (Å)
492			1	-9	10.7	-8.2	9.2
493			2	-8.6	4.2	-7.7	6.3
494			3	-10.1	10.2	-8.7	9.6
495			4	-9.7	10.8	-8.1	11

496 Results for bi-functional sugar-oximes **1** and **2** showed an uniformous low binding affinity for  
497 all OPNAs tested indicating a poor positioning of the oximes inside the gorge of the *hAChE*.  
498 The sugar moiety of compound **1** does not interact with the aromatic residues of the gorge to  
499 give a possible stabilizing interaction, as shown in figure 5. Interestingly, the sugar moiety of  
500 compound **2**, which has a 3 carbon atoms linker, is able to bind between Tyr341 and Tyr337 of  
501 the VX-inhibited *hAChE*. The resulting 4.2 Å distance observed between the oxime oxygen  
502 atom and the phosphorus atom of the phosphorylated *hAChE* is sufficiently short to allow a  
503 possible reactivation of the enzyme by compound **2**. As expected, the binding affinity observed  
504 for tri-functional sugar oximes **3** and **4** appeared to be higher than those observed for **1** and **2**  
505 (Table 1). The triazole moiety of compounds **3** and **4** act as a ligand of the peripheral site by  
506 forming a π stacking interaction with Tyr341, stabilizing the molecule in a productive way.  
507 Overall, the sugar moiety of these new oximes appears to be localized most of the time at the  
508 entrance of the gorge without strong interaction with the peripheral site. In this position, the  
509 sugar moiety cannot interfere with the binding of the oxime moiety down into the gorge,  
510 allowing the oxime oxygen atom to reach a short and productive distance to the phosphorus  
511 atom.



512      Figure 5: Molecular docking of selected oximes in the active site of VX and GB-inhibited human  
 513      acetylcholinesterase (respectively top and bottom panel). The binding energy determined by the scoring function  
 514      of Autodock Vina and the distance between the phosphorus Atom of VX or GB and the oxime oxygen atom are  
 515      indicated in the top left corner each docking pose.

516

### 517      3.3 *In vitro* reactivation of OPNAs phosphorylated hAChE

518      We first determined the half-maximal inhibitory concentration ( $IC_{50}$ ) for compounds **1,2,3** and  
 519      **4** (Table 2). Results showed a generally low affinity of the new sugar-oximes for recombinant  
 520      uninhibited hAChE. Noteworthy, oximes **1** and **2**, which differ only by one carbon atom in the  
 521      alkyl chain between the 3-hydroxypyridinaldoxime and the glucose, displayed a high binding  
 522      affinity difference implying that the length of the linker (i.e., four carbons for oxime **1** versus 3  
 523      carbons for oxime **2**) is a key parameter for the binding of the reactivators to their target. The  
 524      higher flexibility allowed by the four carbons alkyl chain of oxime **1** may prevent the molecule  
 525      to bind tightly to the enzyme. Oximes **3** and **4** also differ by one carbon atom in the length of  
 526      the alkyl chain between the oxime moiety and the triazole (3 carbons for oxime **3** and 4 for  
 527      oxime **4**). The binding affinity of oxime **3** is approximatively three times lower than the affinity  
 528      of oxime **4** which may indicate that the four carbons linker of compound **4** allows a more

529 effective binding of the molecule inside the active site of *hAChE*. Altogether, these results  
 530 displaying a low affinity for native *hAChE*, clearly suggest that oximes **1-4** can be used at high  
 531 concentration without inhibiting *hAChE*.

532  
 533 Table 2: Half maximal inhibitory concentration ( $IC_{50}$ ) for *hAChE*.

	Oxime	$IC_{50}$ $\mu M$
	1	97% at 5 mM
	2	140 $\pm$ 20
	3	1600 $\pm$ 200
	4	580 $\pm$ 10
	HI-6	55 $\pm$ 5
	2-PAM	560 $\pm$ 30
	Obidoxime	640 $\pm$ 70

541 We then determined the reactivation kinetics constants for the selected oximes, as showed in  
 542 table 3. The  $\alpha$  anomer of compound **4** (compound **4'**) and the riboconjugate of compound **4**,  
 543 (compound **5**) were also tested for their reactivation efficacy. Surrogates of VX (NEMP), sarin  
 544 (NIMP) and tabun (NEDPA) as well as an organophosphorus pesticide (paraoxon) were used  
 545 for *hAChE* inhibition, as they give the same phosphoryl moiety on the serine residue as their  
 546 corresponding OPNA.

547 Table 3: Reactivation kinetics of *hAChE* inhibited by nerve agent surrogated and paraoxon by selected oximes.  
 548 *nd*: if [reactivator]  $\ll K_D$ , then there is a linear dependence between  $k_{obs}$  and [reactivator]:  $k_{obs} =$   
 549  $(k_r/K_D)[reactivator]$ . In this case,  $K_r$  and  $K_D$  cannot be determined, but  $k_{r2} = k_r/K_D$  is the slope of the line and can  
 550 be directly obtained by fitting.

OP	Oxime	$k_r$ $min^{-1}$	$K_D$ mM	$k_{r2}$ $mM^{-1}.min^{-1}$
NEMP	<b>1</b>	0.4 $\pm$ 0.1	4 $\pm$ 1	0.1
	<b>2</b>	0.3 $\pm$ 0.01	1 $\pm$ 0.09	0.2
	<b>3</b>	0.5 $\pm$ 0.07	1.5 $\pm$ 0.3	0.3
	<b>4</b>	1 $\pm$ 0.1	1 $\pm$ 0.3	1
	<b>4'</b>	1 $\pm$ 0.02	1 $\pm$ 0.04	1
	<b>5</b>	2.5 $\pm$ 0.2	2.4 $\pm$ 0.4	1.0
	<b>HI-6</b>	0.65 $\pm$ 0.03	0.07 $\pm$ 0.008	9.3
	<b>2-PAM</b>	0.1 $\pm$ 0.01	0.2 $\pm$ 0.06	0.5
NIMP	<b>Obidoxime</b>	0.2 $\pm$ 0.007	0.6 $\pm$ 0.04	0.3
	<b>1</b>	0.2 $\pm$ 0.006	1 $\pm$ 0.08	0.2
	<b>2</b>	0.2 $\pm$ 0.02	2 $\pm$ 0.4	0.1
	<b>3</b>	0.2 $\pm$ 0.01	1.3 $\pm$ 0.2	0.15
	<b>4</b>	0.7 $\pm$ 0.1	2 $\pm$ 0.5	0.4
	<b>4'</b>	0.4 $\pm$ 0.09	2 $\pm$ 0.7	0.2

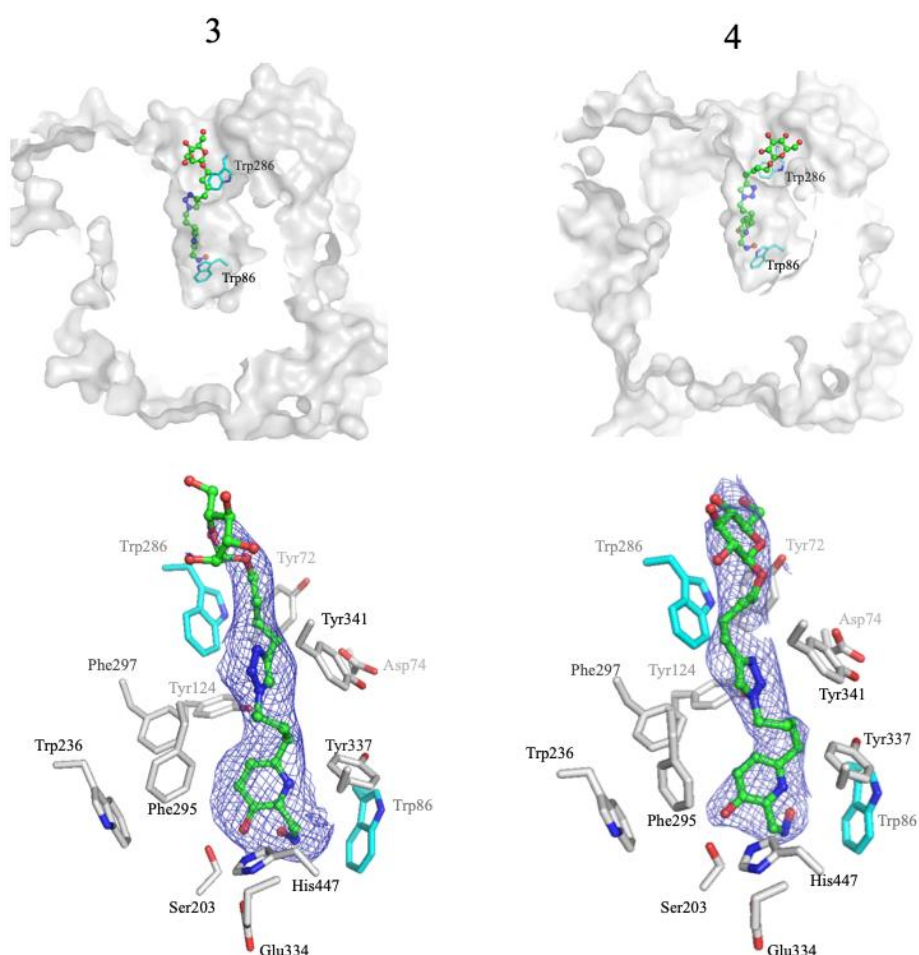
	<b>5</b>	nd	nd	0.2
	<b>HI-6</b>	1 ± 0.2	0.09 ± 0.03	11
	<b>2-PAM</b>	0.24 ± 0.02	0.2 ± 0.03	1.2
	<b>Obidoxime</b>	0.2 ± 0.02	0.5 ± 0.09	0.4
	<b>1</b>	0.1 ± 0.01	1.3 ± 0.2	0.1
	<b>2</b>	0.2 ± 0.02	1.2 ± 0.3	0.2
	<b>3</b>	0.2 ± 0.08	3 ± 1.4	0.07
	<b>4</b>	0.6 ± 0.02	0.9 ± 0.1	0.6
NEDPA	<b>4'</b>	0.5 ± 0.04	0.6 ± 0.1	0.8
	<b>5</b>	0.8 ± 0.2	3 ± 1	0.3
	<b>HI-6</b>	0.05 ± 0.005	0.2 ± 0.04	0.2
	<b>2-PAM</b>	0.15 ± 0.025	0.8 ± 0.2	0.2
	<b>Obidoxime</b>	0.6 ± 0.04	0.3 ± 0.07	2
	<b>1</b>	0.03 ± 0.005	0.5 ± 0.2	0.05
	<b>2</b>	nd	nd	0.2
	<b>3</b>	0.2 ± 0.08	2 ± 0.4	0.2
	<b>4</b>	0.6 ± 0.1	2 ± 0.7	0.3
PARAOXON	<b>4'</b>	nd	nd	0.8
	<b>5</b>	0.6 ± 0.1	2.7 ± 0.7	0.2
	<b>HI-6</b>	0.09 ± 0.009	0.8 ± 0.14	0.1
	<b>2-PAM</b>	0.05 ± 0.006	0.4 ± 0.08	0.1
	<b>Obidoxime</b>	0.3 ± 0.02	0.5 ± 0.09	0.6

552  
553 The results, displayed in table 3, showed a generally low efficacy ( $k_{r2}$ ) of the sugar oximes in  
554 the same range as 2-PAM in all cases, and in the same range of HI-6 (but lower than  
555 obidoxime), for NEDPA and paraoxon phosphorylated hAChE. The low affinity ( $K_D$ ), in the  
556 millimolar range, of these compounds for the phosphorylated hAChE are clearly responsible for  
557 the poor reactivation efficiency. However, the compounds **4**, **4'** and **5** performed better than 2-  
558 PAM and obidoxime for the NEMP-inhibited hAChE, mainly due to the hight reactivation rates  
559 observed. Regarding the NIMP-inhibited hAChE, the sugar oximes are outperformed by HI-6,  
560 2-PAM and obidoxime, and they are slightly better than HI-6 and 2-PAM for NEDPA-inhibited  
561 enzyme. Compound **4'** appeared to reactivate the paraoxon inhibited hAChE better than HI-6,  
562 2-PAM, and obidoxime.

### 563 **3.4 X-ray structures of compounds 3 and 4 in native hAChE**

564 In order to confirm the binding position of the sugar-oximes in the gorge of hAChE, we solved  
565 the structure of the complexes formed by the non-modified hAChE and compound **3** (PDB  
566 7P1P) and **4** (PDB 7P1N) (Figure 6). Data collection and refinement statistics are presented in

567 table S2. An overall view of the binding of compounds **3** and **4** in the gorge of *hAChE* shows  
 568 the binding of the oximes are in a favorable orientation. Indeed, the oxime moiety is located at  
 569 the bottom of the gorge, close to the catalytic serine, and the sugar moiety can be observed  
 570 outside the gorge not interacting with Trp286, thus not interfering with the reactivation reaction.  
 571 A closer view (Figure 6 ; lower panel), illustrates the interactions of compounds **3** and **4** with  
 572 the aromatic aminoacid lining the gorge of the *hAChE*. For both compounds, we can observe  
 573  $\pi$ -stacking interaction between the triazole and the Tyr341, as predicted by molecular docking.

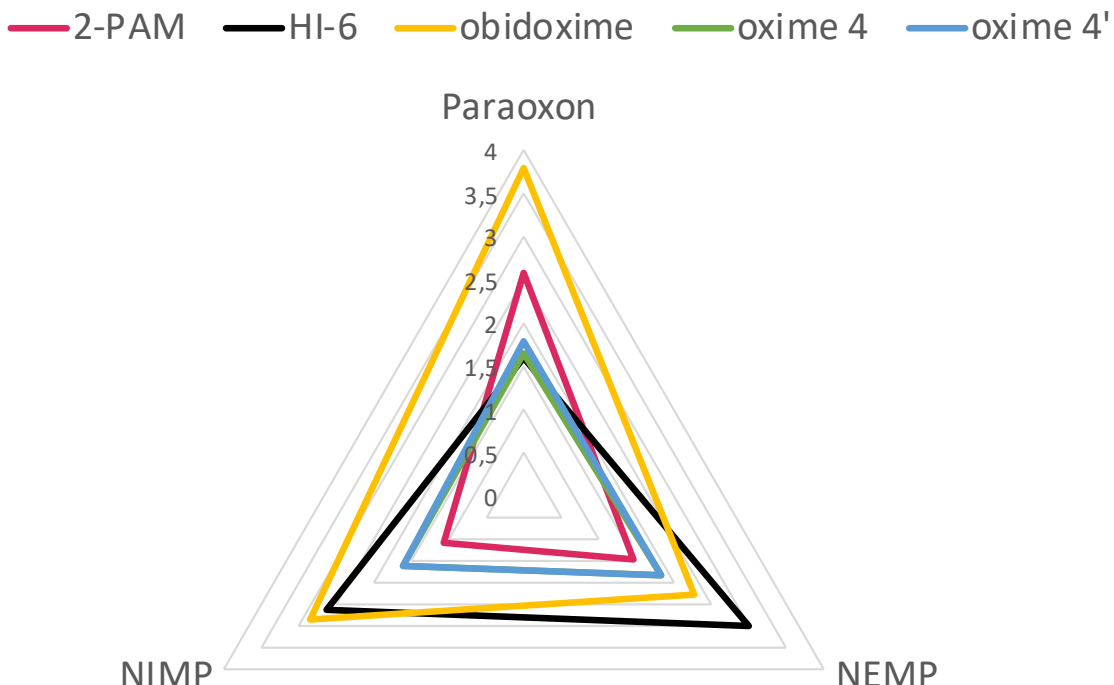


574  
 575 Figure 6 : Views of oxime **3** (PDB 7P1P) and **4** (PDB 7P1N) in complex with *hAChE*.  
 576 Top : Overall view of oximes **3** and **4** location inside the gorge of *hAChE* defined by the solvent accessible surface,  
 577 showing the sugar moiety outside the gorge. Bottom : Closer view of oximes **3** and **4** inside the gorge of *hAChE*.  
 578 A 1- $\sigma$  feature-enhanced map is represented as a blue mesh. Key peripheral (Trp286) and active site (Trp86)  
 579 tryptophan residues are represented in sticks with carbons in cyan.  
 580  
 581  
 582  
 583  
 584

585    3.5    ***In vivo* protective index assessment**

586    In order to determine the *in vivo* efficacy of the new oximes, protective indexes (PI) were  
587    determined for compounds **4** and **4'** at 100 µmol/kg and compared to 2-PAM, HI-6, obidoxime.  
588    Experiments of up-and-down procedure performed on paraoxon, NIMP and NEMP exposure  
589    are presented in Table S3, S4 and S5 respectively and summed up in Figure 7. LD<sub>50</sub> of paraoxon,  
590    NIMP and NEMP were respectively established to 818, 605 and 350 µg/kg. PI of a 100 µmol/kg  
591    i.p. 2-PAM treatment 1 min after paraoxon exposure was previously assessed to 2.58<sup>37</sup>. Alone,  
592    100 µmol/kg of obidoxime gave the most interesting protective spectrum against the three  
593    studied OPs even if HI-6 showed a higher PI than obidoxime in the case of treatment of NEMP  
594    exposure (3.00 vs. 2.06), the lowest protective efficacy of HI-6 against paraoxon exposure (PI  
595    = 1.6) was crippling. It should be noted that oximes **4** and **4'** presented an almost identical and  
596    moderate *in vivo* protection against the three OP exposures.

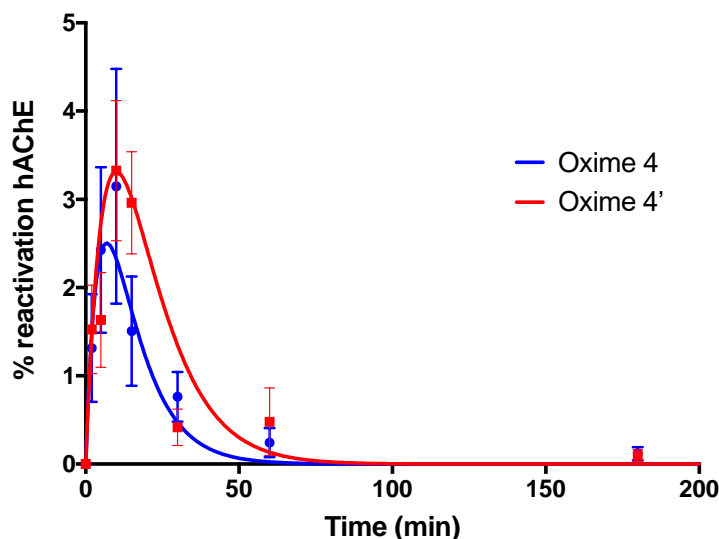
### Protective index without atropine



597    **Figure 7.** Radar representation of PI values of 100 µmol/kg intraperitoneally treatment of 2-PAM, HI-6,  
598    obidoxime, oxime **4** and **4'** one minute after paraoxon, NIMP or NEMP subcutaneous exposure. PI were  
599    determined by the up-and-down method.

600 **3.6 Pharmacokinetic study**

601 Both oximes (**4** and **4'**) exhibited a similar enzymatic reactivation profile with a low  
 602 reactivation percentage at the peak (React max =  $2,5 \pm 0,8\%$  and  $3,3 \pm 0,7\%$  respectively).  
 603 The peak is reached more rapidly for oxime **4** than for oxime **4'** ( $T_{max} = 7,0 \pm 0,0$  vs  $10,0 \pm$   
 604 0,0 min after injection) as shown in Fig. 8. Oxime **4** also persisted for a shorter time than  
 605 oxime **4'** in mice plasma as demonstrated by the MRT value ( $15,0 \pm 0,0$  vs  $20,0 \pm 0,0$  min).



606 **Figure 8.** reactivation of VX-inhibited hAChE by oximes **4** and **4'** in mice plasma. The same dose of 100  
 607  $\mu\text{mol/kg}$  of oxime **4** and **4'** was administered intraperitoneally to mice ( $n = 7$ ). Blood samples were drawn at  
 608 various time points (0, 2, 5, 10, 15, 30, 60 and 180 min) after treatment, and the levels of reactivation of VX-  
 609 phosphorylated hAChE were determined. Values are presented as percentages of maximum reactivation and  
 610 points are means  $\pm$  SEM. Fitting was performed on GraphPad Prism software.

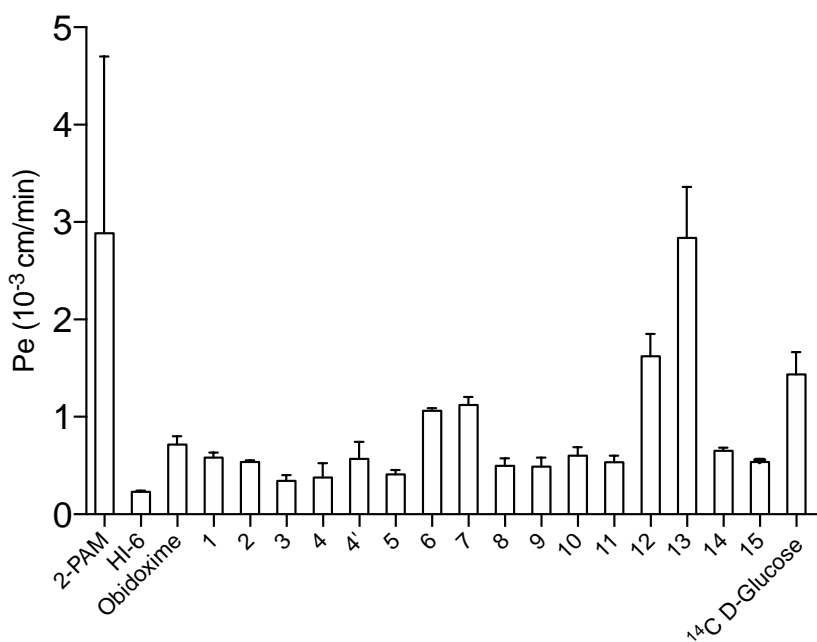
611

612 **Table 4.** Pharmacokinetic data of oximes **4** and **4'**. MRT: mean residence time,  $T_{max}$  and React max  
 613 respectively x and y coordinates of the peak of reactivation of VX-phosphorylated hAChE by oximes **4** and **4'**  
 614 in mice plasma presented in Figure 8, and  $C_{max}$  the peak concentration of oximes **4** and **4'** calculated from  
 615 standard reactivation curves (Figure S1).

	Oxime	MRT (min)	$T_{max}$ (min)	React max (%)	$C_{max}$ ( $\mu\text{M}$ )
	<b>Oxime 4</b>	$15,0 \pm 0,0$	$7,0 \pm 0,0$	$2,5 \pm 0,8$	96,7
	<b>Oxime 4'</b>	$20,0 \pm 0,0$	$10,0 \pm 0,0$	$3,3 \pm 0,7$	145,7

622 **3.7 Blood-brain barrier permeability tests**

623 One aim was to improve the transport of the oximes across the blood-brain barrier (BBB)  
624 endothelial cells to reactivate the central AChE. In order to determine if our sugar oximes are  
625 able to reach the CNS, we evaluated the endothelial permeability coefficients (Pe) of some  
626 gluco- and riboconjugate oximes (compounds **1, 2, 3, 4, 4', 5, 15**) as well as representative  
627 simpler glycoconjugate molecules (compounds **6, 7, 8, 9, 10, 11, 12, 13, 14**) using the human  
628 BBB *in vitro* model. No toxicity was observed in our culture conditions (data not shown).



629 Figure 9: Endothelial permeability coefficients (Pe) of control oximes (2-PAM, HI-6, obidoxime), glycoconjugate  
630 oximes (compounds **1,2,3,4,4',5,15**), gycococonjugate intermediates (compounds **6, 7, 8, 9, 10, 11, 12, 13, 14**) and  
631 <sup>14</sup>C D-glucose. Values are means  $\pm$  SD, n=3-9.

632 Results showed that all the compounds, the conjugate oximes or the simpler glycoconjugate  
633 molecules, had a lower rate of transport through BBB endothelial cells than 2-PAM ( $Pe_{2\text{-PAM}} =$   
634  $2.89 \pm 1.81 \times 10^{-3} \text{ cm} \cdot \text{min}^{-1}$ ) (Figure 9). Only one glycoconjugate without oxime moiety  
635 (compound **13**) exhibited a permeability coefficient in the same range ( $Pe_{13} = 2.83 \pm 0.52 \times 10^{-3}$   
636  $\text{cm} \cdot \text{min}^{-1}$ ). Most of the molecules showed Pe values between those of HI-6 ( $Pe = 0.23 \pm 0.01$   
637  $\times 10^{-3} \text{ cm} \cdot \text{min}^{-1}$ ) and obidoxime ( $Pe = 0.72 \pm 0.08 \times 10^{-3} \text{ cm} \cdot \text{min}^{-1}$ ) that are described to slowly  
638 cross the BBB which is confirmed in our *in vitro* model study (Figure 9).  
639

640 The rate of transport of glycoconjugate oximes (compounds **1**, **2**, **3**, **4**, **4'**, **5**, **15**) has also been  
641 compared to that of  $^{14}\text{C}$  D-glucose which is taken up by a transporter (GLUT-1) so as to  
642 facilitate its crossing through membranes of the endothelial cells. The Pe values of  
643 glycoconjugate oximes (Pe from  $0.34$  to  $0.58 \times 10^{-3} \text{ cm} \cdot \text{min}^{-1}$ , table S6) were two to three-fold  
644 lower than that of glucose ( $\text{Pe}_{\text{glucose}} = 1.43 \pm 0.23 \times 10^{-3} \text{ cm} \cdot \text{min}^{-1}$ ). At this stage, to understand  
645 at which level of the oxime glycoconjugates were no longer supported by the facilitated  
646 diffusion, the Pe values of the simpler glycoconjugate molecules were also evaluated and  
647 compared to that of glucose. None or slight differences were observed between the endothelial  
648 permeability coefficients of the  $^{14}\text{C}$  D-glucose and those of the ribose (compounds **12**, **13**) or  
649 glucose (compounds **6,7**) connected with an additional alkyne moiety bearing carbon chain (3  
650 or 5 additional carbons branched at the anomeric oxygen atom) showing that these molecules  
651 crossed the BBB endothelium in the same way as glucose. The strategy used here, is a first step  
652 to improve the transport of molecules through the BBB. However, when a triazole moiety has  
653 been connected to the additional carbon chain of ribose (compound **14**) or of glucose  
654 (compounds **8, 9, 10, 11, 12**) Pe values showed a three- and two-fold decrease, respectively  
655 demonstrating that the rate of transport through the endothelial cells was slowed down in the  
656 same range as for the gluco- and riboconjugate oximes (Figure 9, Table S6). These results  
657 showed that in the process of the glycoconjugates synthesis, the triazole moiety, required for  
658 the binding of the oximes to *hAChE*, has a detrimental effect on BBB crossing ability, as this  
659 moiety has been shown to restrain the facilitated diffusion through glucose transporters.

660 **4 Discussion/conclusion**

661 Reactivation of the central OP-phosphylated AChE is one of the aims of the newly synthesized  
662 oximes which have been described lately in the literature. An efficient crossing of the BBB  
663 appears to be one major limitation for these numerous new designed oxime reactivators. If  
664 efficient reactivation of peripheral phosphylated *hAChE* is the key for survival after OPNA

exposure, inhibition of central AChE may induce long-term side effects and detrimental neurological disorders. Many design strategies, among which the use of uncharged or glucoconjugated reactivators have been evaluated to overcome this limitation. In this study, we intended to evaluate the combination of these two strategies, and evaluated the ability of a new family of uncharged glucoconjugated 3-hydroxypyridinaldoxime to reactivate inhibited *h*AChE with the goal in mind to take advantage of the glucose transporter system located at the BBB in order to reach the centrally OP-phosphorylated AChE. We thus synthesized simple bi-functional glycoconjugated uncharged reactivators **1** and **2**, which displayed, as expected, low affinity for the phosphorylated *h*AChE and a poor reactivation profile. We also synthesized tri-functional glycoconjugated uncharged oximes **3**, **4**, **4'**and **5** bearing an additional triazole moiety in order to increase the affinity of these oximes for the phosphorylated AChE through binding of the triazole moiety to the peripheral site of the enzyme. An *in-silico* study by molecular docking of bi-functional oximes **1** and **2** and tri-functional oximes **3** and **4** showed a general low binding affinity between -7,7 and -10,1 kcal/mol for VX or GB inhibited *h*AChE. Except for compound **2**, the results showed P-O distances between 9,2 and 11 Å. All together, these *in-silico* results suggested that oximes **1**, **2**, **3** and **4** may reactivate, yet with moderate efficiency the VX or GB-phosphylated *h*AChE. We then evaluated the reactivation efficiency of oximes **1**, **2**, **3**, **4**, and **4'** (the  $\alpha$  anomer of compound **4**) and oxime **5** (the riboconjugated analogue of oxime **4**). The results show a general low binding affinity ( $K_D$ ) in the millimolar range of the sugar oximes for the phosphorylated *h*AChE. This low binding affinity negatively affected the overall reactivation efficacy ( $k_{r2}$ ). It may be due to the presence of the sugar moiety on the oximes, which does not allow the compound to penetrate deep enough inside the gorge of the phosphorylated enzyme for an efficient reactivation. Crystal structures of compounds **3** and **4** have been solved in complex with *h*AChE (PDB 7P1P and 7P1N). Data show that both oximes were able to enter the gorge of the *h*AChE with the 3-hydroxypyridinaldoxime moiety located

690 near the catalytic site, the triazole moiety interacting by  $\pi$ -stacking interactions with Tyr341  
691 and the glucose moiety spanning outside the gorge without unfavorable interactions with amino  
692 acids of the peripheral site. These results showed that compounds **3** and **4** were orientated inside  
693 the gorge in a productive way that may reactivate the inhibited *hAChE*. The presence of the  
694 triazole moiety on oximes **3**, **4**, **4'** and **5** was predicted to improve the affinity of the sugar  
695 oximes for the inhibited enzymes, but results showed a similar low binding affinity in the same  
696 range as compounds **1** and **2**. However, a high enough reactivation kinetics  $k_r$  allows oximes **4**,  
697 **4'** and **5** to be more efficient than 2-PAM and obidoxime to reactivate the NEMP-phosphylated  
698 *hAChE* as well as oximes **4** and **4'** to reactivate NEDPA-phosphylated *hAChE*. The  $\alpha$  anomer  
699 of the oxime **4** (named **4'**) is the only compound to perform better than 2-PAM, HI-6 and  
700 obidoxime for paraoxon phosphylated *hAChE*.

701 Our goal was to design new uncharged oximes that could reach the CNS more efficiently  
702 through the active glucose transporter located at the BBB. In order to evaluate our hypothesis  
703 we determined protective indexes for compounds **4** and **4'** on mice exposed to NIMP, NEMP  
704 and paraoxon. Our results showed that oximes **4** and **4'** display a similar protection profile. The  
705 use of the  $\alpha$  anomer of compound **4** did not improve the protective index. *In vivo* results showed  
706 that both oxime protect as well as HI-6 in mice exposed to paraoxon and appeared to be more  
707 effective than 2-PAM against NIMP and NEMP. Pharmacokinetic studies demonstrated, after  
708 an intraperitoneal injection, the presence of compounds **4** and **4'** in blood during the  
709 experiments but showed that only a low percentage of VX-phosphylated enzymes could be  
710 reactivated. *In-vitro* reactivation studies have shown the low affinity of the sugar-oximes for  
711 the phosphylated *hAChE* and, therefore, their moderate reactivation capabilities. We can  
712 hypothesize that the low protective indexes recorded in this study may be improved by  
713 administering a higher dose of oxime in adequacy with the compound properties : interestingly,  
714 contrary to HI-6, these oximes poorly inhibit native *hAChE* and can thus be used at a higher

715 dose.

716 To evaluate the ability of our sugar oximes conjugates to cross the BBB we determined the  
717 endothelial permeability coefficients of gluco- and riboconjugate oximes (**1, 2, 3, 4, 4', 5, 15**)  
718 as well as simpler glycoconjugated molecules (compounds **6, 7, 8, 9, 10, 11, 12, 13, 14**) using  
719 the human BBB *in vitro* model (Figure 9). Our results showed that the designed sugar oximes  
720 do not cross the BBB at the same transport rate as glucose, implying a structural restrain from  
721 our compounds. 2-PAM has the highest transport rate than any other evaluated oximes, but the  
722 Pe for oxime **1, 2, 3, 4, 4'** and **5** is higher than the Pe for HI-6 and slightly lower than the Pe for  
723 obidoxime. However, we were disappointed to observe that the presence of the triazole moiety  
724 on tri-functional oximes **3, 4, 4', 5**, incorporated to increase the affinity of these compounds for  
725 phosphorylated *hAChE*, as well as its presence in simpler glycoconjugated molecules such as **8,**  
726 **9, 10, 11** and **14** reduces the transport rate through the BBB which may negatively impact the  
727 protective index determined in our *in vivo* experiments.

728 In summary, we designed a new family of uncharged oximes glycoconjugates to combine two  
729 strategies to reach the CNS more efficiently through the use of non-permanently charges oximes  
730 and taking advantage of an active glucose transport system to improve the protection of oxime-  
731 based reactivators against neurotoxic organophosphorus poisoning. Our study showed that our  
732 compounds perform roughly as the oximes currently used across the world but highlights the  
733 structural restraints which apply to oximes targeting the glucose transport system: addition of  
734 an additional aromatic moiety to improve binding of the oximes to phosphorylated *hAChE*  
735 negatively impacts their BBB crossing ability. Based on this work, new sugar-oximes could be  
736 designed using other moieties than triazoles to bind efficiently phosphorylated *hAChE*, and  
737 probably longer side chains between the first two components of these tri-functional  
738 reactivators (sugar / AChE binding moiety / oxime), synthesized in order to use efficiently this  
739 glucose transport system of the BBB to reach the central OP-phosphylated AChE.

740    **5 Acknowledgments**

741    The mass spectrometer of the SMART (Spectrometrie de Masse de l'ARTois) core facilities  
742    used in this study was funded by the European and Regional Development Fund (ERDF),  
743    the conseil régional Hauts-de-France and Artois University (France). The authors warmly  
744    thank the technical support collaboration from Sophie Duban-Deweir and Johan Hachani  
745    for the help with the LC-MS/MS. This study and salary of CC, NP and PW were founded  
746    by the ANR grant "CNS antidote" (ANR-17-CE39-0012) and ANR grant "ReCNS-AChE"  
747    (ANR-13-ASTR-0002). The authors also gratefully acknowledge the Direction Générale de  
748    l'Armement (DGA) and Service de Santé des Armées (SSA) of the French Ministry of  
749    Armed Forces for sustained financial support to O.D.S, A.G.C, A.S.H, C.C, A.J.G, M.T,  
750    F.N, and J.D (grant NBC-5-C-4210). This work has been partially supported by INSA Rouen  
751    Normandy, University of Rouen Normandy, the Centre National de la Recherche  
752    Scientifique (CNRS), EFRD, Labex SynOrg (ANR-11-LABX-0029), the graduate school  
753    for research XI-Chem (ANR-18-EURE-0020 XL CHEM), and by Region Normandie.

754    **6 References**

1. Nakagawa, T., Tu, A. T., Murders with VX: Aum Shinrikyo in Japan and the assassination of Kim Jong-Nam in Malaysia *Forensic Toxicol* **2018**, vol. 36, n°2, p. 542 - 544.
2. Chai, P. R.; Hayes, B. D.; Erickson, T. B.; Boyer, E. W., Novichok agents: a historical, current, and toxicological perspective. *Toxicol Commun* **2018**, 2 (1), 45-48.
3. Sidell, F. R., Soman and sarin: clinical manifestations and treatment of accidental poisoning by organophosphates. *Clin Toxicol* **1974**, 7 (1), 1-17.
4. Jokanovic, M., Medical treatment of acute poisoning with organophosphorus and carbamate pesticides. *Toxicol Lett* **2009**, 190 (2), 107-15.
5. Melchers, B. P.; Philippens, I. H.; Wolthuis, O. L., Efficacy of HI-6 and HLo-7 in preventing incapacitation following nerve agent poisoning. *Pharmacol Biochem Behav* **1994**, 49 (4), 781-8.
6. Lorke, D. E.; Kalasz, H.; Petroianu, G. A.; Tekes, K., Entry of oximes into the brain: a review. *Curr Med Chem* **2008**, 15 (8), 743-53.
7. Kassa, J., Review of oximes in the antidotal treatment of poisoning by organophosphorus nerve agents. *J Toxicol Clin Toxicol* **2002**, 40 (6), 803-16.
8. Mercey, G.; Verdelet, T.; Renou, J.; Kliachyna, M.; Baati, R.; Nachon, F.; Jean, L.; Renard, P. Y., Reactivators of acetylcholinesterase inhibited by organophosphorus nerve agents. *Acc Chem Res* **2012**, 45 (5), 756-66.
9. Worek, F.; Thiermann, H.; Wille, T., Organophosphorus compounds and oximes: a critical review. *Arch Toxicol* **2020**, 94 (7), 2275-2292.
10. Shih, T.-M., Koplovitz, I., Kan, R.K., McDonough, J.H., In search of an effective in vivo reactivator for organophosphorus nerve agent-inhibited acetylcholinesterase in the central nervous system *Advanced Studies in Biology* **2012**, Vol. 4 (no. 9-12), 451-478.
11. Sit, R. K.; Radic, Z.; Gerardi, V.; Zhang, L.; Garcia, E.; Katalinic, M.; Amitai, G.; Kovarik, Z.; Fokin, V. V.; Sharpless, K. B.; Taylor, P., New structural scaffolds for centrally acting oxime reactivators of phosphorylated cholinesterases. *J Biol Chem* **2011**, 286 (22), 19422-30.
12. Mercey, G.; Verdelet, T.; Saint-Andre, G.; Gillon, E.; Wagner, A.; Baati, R.; Jean, L.; Nachon, F.; Renard, P. Y., First efficient uncharged reactivators for the dephosphylation of poisoned human acetylcholinesterase. *Chem Commun (Camb)* **2011**, 47 (18), 5295-7.
13. Zorbaz, T.; Braiki, A.; Marakovic, N.; Renou, J.; de la Mora, E.; Macek Hrvat, N.; Katalinic, M.; Silman, I.; Sussman, J. L.; Mercey, G.; Gomez, C.; Mugeot, R.; Perez, B.; Baati, R.; Nachon, F.; Weik, M.; Jean, L.; Kovarik, Z.; Renard, P. Y., Potent 3-Hydroxy-2-

- 790 Pyridine Aldoxime Reactivators of Organophosphate-Inhibited Cholinesterases with Predicted  
791 Blood-Brain Barrier Penetration. *Chemistry* **2018**, *24* (38), 9675-9691.
- 792 14. Calas, A. G.; Dias, J.; Rousseau, C.; Arboleas, M.; Touvrey-Loiodice, M.; Mercey,  
793 G.; Jean, L.; Renard, P. Y.; Nachon, F., An easy method for the determination of active  
794 concentrations of cholinesterase reactivators in blood samples: Application to the efficacy  
795 assessment of non quaternary reactivators compared to HI-6 and pralidoxime in VX-poisoned  
796 mice. *Chem Biol Interact* **2017**, *267*, 11-16.
- 797 15. Santoni, G.; de Sousa, J.; de la Mora, E.; Dias, J.; Jean, L.; Sussman, J. L.; Silman,  
798 I.; Renard, P. Y.; Brown, R. C. D.; Weik, M.; Baati, R.; Nachon, F., Structure-Based  
799 Optimization of Nonquaternary Reactivators of Acetylcholinesterase Inhibited by  
800 Organophosphorus Nerve Agents. *J Med Chem* **2018**, *61* (17), 7630-7639.
- 801 16. Heldman, E.; Ashani, Y.; Raveh, L.; Rachaman, E. S., Sugar conjugates of pyridinium  
802 aldoximes as antidotes against organophosphate poisoning. *Carbohydr Res* **1986**, *151*, 337-47.
- 803 17. Cornford, E. M.; Hyman, S., Localization of brain endothelial luminal and abluminal  
804 transporters with immunogold electron microscopy. *NeuroRx* **2005**, *2* (1), 27-43.
- 805 18. Garcia, G. E.; Campbell, A. J.; Olson, J.; Moorad-Doctor, D.; Morthole, V. I., Novel  
806 oximes as blood-brain barrier penetrating cholinesterase reactivators. *Chem Biol Interact* **2010**,  
807 *187* (1-3), 199-206.
- 808 19. Viayna, E.; Coquelle, N.; Cieslikiewicz-Bouet, M.; Cisternas, P.; Oliva, C. A.;  
809 Sanchez-Lopez, E.; Ettcheto, M.; Bartolini, M.; De Simone, A.; Ricchini, M.; Rendina, M.;  
810 Pons, M.; Firuzi, O.; Perez, B.; Sasó, L.; Andrisano, V.; Nachon, F.; Brazzolotto, X.; Garcia,  
811 M. L.; Camins, A.; Silman, I.; Jean, L.; Inestrosa, N. C.; Colletier, J. P.; Renard, P. Y.;  
812 Munoz-Torrero, D., Discovery of a Potent Dual Inhibitor of Acetylcholinesterase and  
813 Butyrylcholinesterase with Antioxidant Activity that Alleviates Alzheimer-like Pathology in  
814 Old APP/PS1 Mice. *J Med Chem* **2021**, *64* (1), 812-839.
- 815 20. Oukoloff, K.; Coquelle, N.; Bartolini, M.; Naldi, M.; Le Guevel, R.; Bach, S.;  
816 Josselin, B.; Ruchaud, S.; Catto, M.; Pisani, L.; Denora, N.; Iacobazzi, R. M.; Silman, I.;  
817 Sussman, J. L.; Buron, F.; Colletier, J. P.; Jean, L.; Routier, S.; Renard, P. Y., Design,  
818 biological evaluation and X-ray crystallography of nanomolar multifunctional ligands targeting  
819 simultaneously acetylcholinesterase and glycogen synthase kinase-3. *Eur J Med Chem* **2019**,  
820 *168*, 58-77.
- 821 21. Trott, O.; Olson, A. J., AutoDock Vina: improving the speed and accuracy of docking  
822 with a new scoring function, efficient optimization, and multithreading. *J Comput Chem* **2010**,  
823 *31* (2), 455-61.
- 824 22. de Koning, M. C.; Joosen, M. J. A.; Worek, F.; Nachon, F.; van Grol, M.; Klaassen,  
825 S. D.; Alkema, D. P. W.; Wille, T.; de Bruijn, H. M., Application of the Ugi Multicomponent  
826 Reaction in the Synthesis of Reactivators of Nerve Agent Inhibited Acetylcholinesterase. *J Med  
827 Chem* **2017**, *60* (22), 9376-9392.
- 828 23. Zueva, I.; Dias, J.; Lushchekina, S.; Semenov, V.; Mukhamedyarov, M.; Pashirova,  
829 T.; Babaev, V.; Nachon, F.; Petrova, N.; Nurullin, L.; Zakharova, L.; Ilyin, V.; Masson, P.;  
830 Petrov, K., New evidence for dual binding site inhibitors of acetylcholinesterase as improved  
831 drugs for treatment of Alzheimer's disease. *Neuropharmacology* **2019**, *155*, 131-141.
- 832 24. Carletti, E.; Li, H.; Li, B.; Ekstrom, F.; Nicolet, Y.; Loiodice, M.; Gillon, E.;  
833 Froment, M. T.; Lockridge, O.; Schopfer, L. M.; Masson, P.; Nachon, F., Aging of  
834 cholinesterases phosphorylated by tabun proceeds through O-dealkylation. *J Am Chem Soc* **2008**,  
835 *130* (47), 16011-20.
- 836 25. Ellman, G. L.; Courtney, K. D.; Andres, V., Jr.; Feather-Stone, R. M., A new and rapid  
837 colorimetric determination of acetylcholinesterase activity. *Biochem Pharmacol* **1961**, *7*, 88-  
838 95.
- 839 26. Kabsch, W., Xds. *Acta Crystallogr D Biol Crystallogr* **2010**, *66* (Pt 2), 125-32.

- 840 27. McCoy, A. J.; Grosse-Kunstleve, R. W.; Adams, P. D.; Winn, M. D.; Storoni, L. C.;  
841 Read, R. J., Phaser crystallographic software. *J Appl Crystallogr* **2007**, *40* (Pt 4), 658-674.
- 842 28. Emsley, P.; Lohkamp, B.; Scott, W. G.; Cowtan, K., Features and development of  
843 Coot. *Acta Crystallogr D Biol Crystallogr* **2010**, *66* (Pt 4), 486-501.
- 844 29. Adams, P. D.; Afonine, P. V.; Bunkoczi, G.; Chen, V. B.; Davis, I. W.; Echols, N.;  
845 Headd, J. J.; Hung, L. W.; Kapral, G. J.; Grosse-Kunstleve, R. W.; McCoy, A. J.; Moriarty,  
846 N. W.; Oeffner, R.; Read, R. J.; Richardson, D. C.; Richardson, J. S.; Terwilliger, T. C.;  
847 Zwart, P. H., PHENIX: a comprehensive Python-based system for macromolecular structure  
848 solution. *Acta Crystallogr D Biol Crystallogr* **2010**, *66* (Pt 2), 213-21.
- 849 30. Kwon, Y., Handbook of Essential Pharmacokinetics, Pharmacodynamics and Drug  
850 Metabolism for Industrial Scientists. *Springer: Boston, MA, USA 2007*, *p 1 online resource*  
851 (302 p.) (online resource (302 p.)).
- 852 31. Rispin, A.; Farrar, D.; Margosches, E.; Gupta, K.; Stitzel, K.; Carr, G.; Greene, M.;  
853 Meyer, W.; McCall, D., Alternative methods for the median lethal dose (LD(50)) test: the up-  
854 and-down procedure for acute oral toxicity. *ILAR J* **2002**, *43* (4), 233-43.
- 855 32. Cecchelli, R.; Aday, S.; Sevin, E.; Almeida, C.; Culot, M.; Dehouck, L.; Coisne, C.;  
856 Engelhardt, B.; Dehouck, M. P.; Ferreira, L., A stable and reproducible human blood-brain  
857 barrier model derived from hematopoietic stem cells. *PLoS One* **2014**, *9* (6), e99733.
- 858 33. Pedroso, D. C.; Tellechea, A.; Moura, L.; Fidalgo-Carvalho, I.; Duarte, J.; Carvalho,  
859 E.; Ferreira, L., Improved survival, vascular differentiation and wound healing potential of stem  
860 cells co-cultured with endothelial cells. *PLoS One* **2011**, *6* (1), e16114.
- 861 34. Yan, W.; Zhang, L.; Lv, F.; Moccia, M.; Carlomagno, F.; Landry, C.; Santoro, M.;  
862 Gosselet, F.; Frett, B.; Li, H. Y., Discovery of pyrazolo-thieno[3,2-d]pyrimidinylamino-phenyl  
863 acetamides as type-II pan-tropomyosin receptor kinase (TRK) inhibitors: Design, synthesis,  
864 and biological evaluation. *Eur J Med Chem* **2021**, *216*, 113265.
- 865 35. Bittner, A.; Gosselet, F.; Sevin, E.; Dehouck, L.; Ducray, A. D.; Gaschen, V.; Stoffel,  
866 M. H.; Cho, H.; Mevissen, M., Time-Dependent Internalization of Polymer-Coated Silica  
867 Nanoparticles in Brain Endothelial Cells and Morphological and Functional Effects on the  
868 Blood-Brain Barrier. *Int J Mol Sci* **2021**, *22* (4).
- 869 36. Paul, A.; Huber, A.; Rand, D.; Gosselet, F.; Cooper, I.; Gazit, E.; Segal, D.,  
870 Naphthoquinone-Dopamine Hybrids Inhibit alpha-Synuclein Aggregation, Disrupt Preformed  
871 Fibrils, and Attenuate Aggregate-Induced Toxicity. *Chemistry* **2020**, *26* (69), 16486-16496.
- 872 37. Calas, A. G.; Hanak, A. S.; Jaffre, N.; Nervo, A.; Dias, J.; Rousseau, C.; Courageux,  
873 C.; Brazzolotto, X.; Villa, P.; Obrecht, A.; Goossens, J. F.; Landry, C.; Hachani, J.; Gosselet,  
874 F.; Dehouck, M. P.; Yerri, J.; Kliachyna, M.; Baati, R.; Nachon, F., Efficacy Assessment of  
875 an Uncharged Reactivator of NOP-Inhibited Acetylcholinesterase Based on Tetrahydroacridine  
876 Pyridine-Aldoxime Hybrid in Mouse Compared to Pralidoxime. *Biomolecules* **2020**, *10* (6).
- 877 38. Dehouck, M. P.; Jolliet-Riant, P.; Bree, F.; Fruchart, J. C.; Cecchelli, R.; Tillement,  
878 J. P., Drug transfer across the blood-brain barrier: correlation between in vitro and in vivo  
879 models. *J Neurochem* **1992**, *58* (5), 1790-7.
- 880 39. Santa-Maria, A. R.; Heymans, M.; Walter, F. R.; Culot, M.; Gosselet, F.; Deli, M.  
881 A.; Neuhaus, W., Transport Studies Using Blood-Brain Barrier In Vitro Models: A Critical  
882 Review and Guidelines. *Handb Exp Pharmacol* **2020**.
- 883 40. Tietze, L. F., Bothe, U., Ortho-Carboranyl Glycosides of Glucose, Mannose, Maltose  
884 and Lactose for Cancer Treatment by Boron Neutron-Capture Therapy. . *Chemistry – A  
885 European Journal* **1998**, *4*, 1179–1183.
- 886 41. Zorbaz, T.; Misetic, P.; Probst, N.; Zunec, S.; Zandona, A.; Mendes, G.; Micek, V.;  
887 Macek Hrvat, N.; Katalinic, M.; Braiki, A.; Jean, L.; Renard, P. Y.; Gabelica Markovic, V.;  
888 Kovarik, Z., Pharmacokinetic Evaluation of Brain Penetrating Morpholine-3-hydroxy-2-

- 889 pyridine Oxime as an Antidote for Nerve Agent Poisoning. *ACS Chem Neurosci* **2020**, *11* (7),  
890 1072-1084.
- 891 42. Mandal, P. K. D., P. ; Roy, S.C. , A mild and efficient method for selective cleavage of  
892 ketals and acetals using lithium chloride in water - dimethyl sulfoxide. *Tetrahedron Lett* **1997**,  
893 *38*, 7271–7274.
- 894 43. Teyssot, M. L. N., L.; Canet, J.L.; Cisnetti, F.; Chevry, A.; Gautier, A. , Aromatic  
895 nitrogen donors for efficient copper(I)-NHC CuAAC under reductant-free conditions.  
896 *European J. Org. Chem* **2010**, 3507–3515.
- 897